

WL-TR-97-4034

MATERIALS PROCESSING TECHNOLOGY



Douglas R. Barker
Venkat Seetharaman, Ph.D.
Robert L. Goetz
UES, Inc.
4401 Dayton-Xenia Road
Dayton, OH 45432-1894

December 1996

Final Report for the Period: 1 April 1992 to 1 December 1996

Approved for public release; distribution unlimited.

19980505 020

MATERIALS DIRECTORATE
WRIGHT LABORATORY
AIR FORCE MATERIEL COMMAND
WRIGHT-PATTERSON AIR FORCE BASE, OHIO 45433-7734

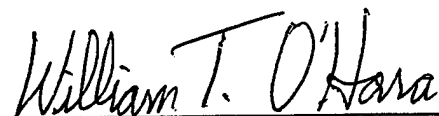
19980505 020

NOTICE

WHEN GOVERNMENT DRAWINGS, SPECIFICATIONS, OR OTHER DATA ARE USED FOR ANY PURPOSE OTHER THAN IN CONNECTION WITH A DEFINITELY GOVERNMENT-RELATED PROCUREMENT, THE UNITED STATES GOVERNMENT INCURS NO RESPONSIBILITY OR ANY OBLIGATION WHATSOEVER. THE FACT THAT THE GOVERNMENT MAY HAVE FORMULATED OR IN ANY WAY SUPPLIED THE SAID DRAWINGS, SPECIFICATIONS, OR OTHER DATA, IS NOT TO BE REGARDED BY IMPLICATION OR OTHERWISE IN ANY MANNER CONSTRUED, AS LICENSING THE HOLDER OR ANY OTHER PERSON OR CORPORATION, OR AS CONVEYING ANY RIGHTS OR PERMISSION TO MANUFACTURE, USE, OR SELL ANY PATENTED INVENTION THAT MAY IN ANY WAY BE RELATED THERETO.

THIS REPORT IS RELEASABLE TO THE NATIONAL TECHNICAL INFORMATION SERVICE (NTIS). AT NTIS, IT WILL BE AVAILABLE TO THE GENERAL PUBLIC, INCLUDING FOREIGN NATIONS.

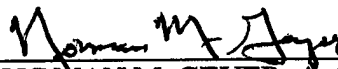
THIS TECHNICAL REPORT HAS BEEN REVIEWED AND IS APPROVED FOR PUBLICATION.



WILLIAM T. O'HARA, Project Engineer
Metals Development & Materials
Processing Branch
Metals, Ceramics & NDE Division



KATHERINE A. STEVENS, Actg Chief
Metals Development & Materials
Processing Branch
Metals, Ceramics & NDE Division



NORMAN M. GEYER, Actg Asst Chief
Metals, Ceramics & Nondestructive
Evaluation Division
Materials and Manufacturing Directorate

IF YOUR ADDRESS HAS CHANGED, IF YOU WISH TO BE REMOVED FROM OUR MAILING LIST, OR IF THE ADDRESSEE IS NO LONGER EMPLOYED BY YOUR ORGANIZATION, PLEASE NOTIFY, AFRL/MLLM, WRIGHT-PATTERSON AFB OH 45433-7817 TO HELP US MAINTAIN A CURRENT MAILING LIST.

DO NOT RETURN COPIES OF THIS REPORT UNLESS CONTRACTUAL OBLIGATIONS OR NOTICE ON A SPECIFIC DOCUMENT REQUIRES ITS RETURN.

REPORT DOCUMENTATION PAGEFORM APPROVED
OMB NO. 0704-0188

Public reporting burden for this collection of information is estimated to average 1 hour per response, including the time for reviewing instructions, searching existing data sources, gathering and maintaining the data needed, and completing and reviewing the collection of information. Send comments regarding this burden estimate or any other aspect of this collection of information, including suggestions for reducing this burden, to Washington Headquarters Services, Directorate for Information Operations and Reports, 1215 Jefferson Davis Highway, Suite 1204, Arlington, VA 22202-4302 and to the Office of Management and Budget, Paperwork Reduction Project (0704-0188), Washington, DC 20503.

1. AGENCY USE ONLY (Leave blank)		2. REPORT DATE DEC 1996	3. REPORT TYPE AND DATES COVERED FINAL 04 /01/92--12/01/96	
4. TITLE AND SUBTITLE MATERIALS PROCESSING TECHNOLOGY			5. FUNDING NUMBERS C F33615-92-C-5900 PE 62102 PR 2420 TA 03 WU 02	
6. AUTHOR(S) DOUGLAS R. BARKER, VENKAT SEETHARAMAN, PH.D., ROBERT L. GOETZ				
7. PERFORMING ORGANIZATION NAMES(S) AND ADDRESS(ES) UES, INC. 4401 DAYTON-XENIA ROAD DAYTON, OH 45432-1894			8. PERFORMING ORGANIZATION REPORT NUMBER	
9. SPONSORING/MONITORING AGENCY NAMES(ES) AND ADDRESS(ES) MATERIALS DIRECTORATE WRIGHT LABORATORY AIR FORCE MATERIEL COMMAND WRIGHT-PATTERSON AFB OH 45433-7734 POC: William T. O'Hara, WL/MLLM, 9387-255-1995			10. SPONSORING/MONITOR- ING AGENCY REPORT NUMBER WL-TR-97-4034	
11. SUPPLEMENTARY NOTES				
12a. DISTRIBUTION/AVAILABILITY STATEMENT APPROVED FOR PUBLIC RELEASE; DISTRIBUTION IS UNLIMITED			12b. DISTRIBUTION CODE	
13. ABSTRACT (Maximum 200 words) The objectives of this program were: (1) to investigate and determine the processing conditions required to achieve desired microstructures and mechanical properties in advanced aerospace materials, (2) to implement and use analytical models for process design in the Materials Processing Laboratory, (3) to validate analytical models by physical modeling, and (4) to create a center of excellence for materials processing. Primary emphasis was given to composites and high temperature materials used in advanced engines and structures. Materials of various types and compositions were studied. In several cases, a full fledged Processing Science approach was utilized, in which the material was fully characterized in terms of microstructural and flow behavior, the proposed processing method was modeled analytically, the actual processing was carried out in the Materials Processing Laboratory (MPL) and the analytical model was validated with experimental measurements. In other cases, some of these steps were eliminated when the material or process was well understood.				
14. SUBJECT TERMS Processing, High Temperature Materials, Process Modeling, Microstructure, Extrusion, Forging, Rolling, Casting			15. NUMBER OF PAGES 108	16. PRICE CODE
17. SECURITY CLASSIFICATION OF REPORT UNCLASSIFIED	18. SECURITY CLASSIFICATION OF THIS PAGE UNCLASSIFIED	19. SECURITY CLASSIFICATION OF ABSTRACT UNCLASSIFIED	20. LIMITATION OF ABSTRACT SAR	

TABLE OF CONTENTS

1. INTRODUCTION.....	1
2. RESEARCH ON ANALYTICAL AND PHYSICAL MODELING OF UNIT PROCESSES	2
2.1 PROCESSING OF ADVANCED TITANIUM ALUMINIDE ALLOYS	2
2.1.1 <i>Extrusion, Forging and Rolling of Gamma TiAl.....</i>	<i>2</i>
2.1.2 <i>Microstructure Development in Wrought Gamma Titanium Aluminide Alloys During Heat Treatments ...</i>	<i>8</i>
2.1.3 <i>Deformation and Fracture of Orthorhombic Titanium Aluminide Sheets</i>	<i>13</i>
2.1.4 <i>Fracture and Hot Workability of Gamma TiAl Alloys</i>	<i>16</i>
2.1.5 <i>Directional Solidification of a Ti-48Al-2Nb-2Cr Alloy.....</i>	<i>18</i>
2.1.6 <i>Plastic Flow and Phase Stability in Orthorhombic Alloys.....</i>	<i>21</i>
2.2 PACK ROLLING OF SINGLE CRYSTAL NICKEL BASE SUPERALLOYS.....	24
2.3 RAPID CONSOLIDATION OF CONTINUOUSLY REINFORCED MMCs	27
2.4 DESIGN OF CONSOLIDATION PRACTICES FROM FOIL/FIBER/FOIL LAY-UPS	31
2.5 NOVEL PROCESSING METHODS	35
2.5.1 <i>Equal Channel Angular Extrusion (ECAE)</i>	<i>35</i>
2.5.2 <i>Graded Microstructures by Induction Heating.....</i>	<i>35</i>
2.5.3 <i>Smart Forging.....</i>	<i>36</i>
2.5.4 <i>Controlled Dwell Extrusion</i>	<i>36</i>
2.6 MICROSTRUCTURE EVOLUTION USING CELLULAR AUTOMATA.....	38
2.7 ELASTIC/PLASTIC FEM MODELING OF TENSILE AND FRACTURE TEST METHODS	41
2.8 EVALUATION OF HTC IN DEFORMATION & SOLIDIFICATION	43
3. MODELING TASKS.....	46
3.1 MMC CONSOLIDATION MODELING AND EXPERIMENTAL VALIDATION	46
3.2 TENSILE TEST SIMULATION	46
3.3 STRESS ANALYSIS OF TiAl INGOTS DURING REHEATING.....	47
3.4 NOTCHED TENSILE TEST SIMULATION	47
3.5 NOTCHED FOUR POINT BEND TEST SPECIMEN SIMULATION	48
3.6 UNIAXIAL UPSETTING OF A POROUS ALUMINA CYLINDER USING ALPID-PM.....	48
3.7 HEAT TRANSFER MODELING OF MMC LAY-UPS USING ALAM 1-D MODEL.....	49
3.8 CONTROLLED DWELL CANNED FORGING	50
3.9 AL-Li ROLLING	51
3.10 COOLING CURVE PREDICTION OF AL-Li CUBE USING ANTAREST™ 3D AND LUMPED PARAMETER MODEL.....	51

3.11 THE EFFECT OF CAN SHIELDING DURING PM HIP CONSOLIDATION.....	51
3.12 GM LCB Ti FORGING/EXTRUSION SIMULATION FOR C.V. JOINT	52
3.13 EXTRUSION/FORGING SIMULATION OF CANNED TIAL FOR GE/AF CRDA TITLED, "TEXTURE DEVELOPMENT DURING GAMMA PROCESSING"	53
3.14 SHEET TENSILE TEST SIMULATION EVALUATING SPECIMEN SHAPE AND DEFORMATION	56
3.15 EQUAL CHANNEL ANGULAR EXTRUSION (ECAE) MODELING.....	56
3.16 TEMPERATURE PREDICTION DURING MMC FORGING BASED ON EARLIER WORK.....	58
3.17 CONTROLLED DWELL G2 TIAL EXTRUSION SIMULATIONS	59
3.18 CONTROLLED DWELL EXTRUSION AND PLOTTING OF A γ -TIAL FOR THE AF/GEAE PROGRAM, "EFFICIENT PROCESSING OF GAMMA TITANIUM ALUMINIDES"	61
3.19 VALVE FORGING OF CANNED/TIAL.....	63
3.20 HEAT TRANSFER MODELING OF A SUBSCALE TIAL DISK DURING HEATING AND COOLING.....	64
3.21 SUBSCALE DISK FORGING	64
3.22 DEFORMATION OF SINGLE POWDER PARTICLE USING ANTARES 3D.....	65
3.23 PUBLICATIONS AND PATENTS ON MODELING TASKS.....	65
4. COOPERATIVE PROJECTS.....	68
4.1 GAMMA CONVERSION PROGRAM	68
4.2 GENERAL MOTORS CONSTANT VELOCITY JOINT PROJECT	69
4.3 Ti-Sn COOPERATIVE PROJECT WITH NAVAL SURFACE WARFARE CENTER	71
4.4 INCO 625 SHEET ROLLING FOR F118-101 TEST PROGRAM	72
4.5 SILVER-GRAPHITE EXTRUSION FOR CMW, INC.	72
4.6 TANTALUM ALLOY EXTRUSIONS FOR DEPARTMENT OF ENERGY PROGRAM	73
4.7 EXTRUSION OF ODS MOLYBDENUM FOR USDOE & PITTSBURGH MATERIALS TECHNOLOGY INC.	74
4.8 EXTRUSION OF HIGH TEMPERATURE ALLOYS FOR USDOE & PITTSBURGH MATERIALS TECHNOLOGY INC.	76
4.9 Co-EXTRUSION OF DUAL ALLOY BILLETS FOR DYNAMET	77
4.10 ROLLING PROGRAM WITH OHIO ADVANCED TECHNOLOGY CENTER.....	78
5. PROCESSING OF MATERIALS.....	79
5.1 EXTRUSION.....	79
5.2 FORGING	81
5.3 ROLLING.....	82
5.4 MECHANICAL TESTING.....	83
5.5 EVACUATION AND DEGASSING.....	84
5.6 VACUUM ARC MELTING (BUTTON MELTS).....	85
5.7 VACUUM INDUCTION MELTING (VIM).....	86
5.8 HEAT TREATMENT.....	87
5.9 WELDING AND FABRICATION	88

6. FOUNDRY MOVE	89
7. OPERATION OF MATERIALS PROCESSING LABORATORY	91
7.1 ISOTHERMAL FORGING CHAMBER AND TOOLING	91
7.2 200 KIP TEST FRAME AND HEAT TRANSFER MEASUREMENT SYSTEM	93
7.3 55 KIP TEST FRAME AND HOT COMPRESSION TEST SETUP	93
7.4 SALT POT FURNACES.....	94
7.5 COMPUTERIZED EXTRUSION DATABASE.....	94

LIST OF TABLES

Table 3-1: G2 TiAl, Controlled Dwell Simulation Parameters	60
Table 5-1: Summary of Extrusions.....	80
Table 5-2: Summary of Forging Operations	81
Table 5-3: Summary of Rolling Operations	82
Table 5-4: Summary of Mechanical Testing.....	83
Table 5-5: Summary of Evacuation, Outgassing and Sealing Operations	84
Table 5-6: Summary of Vacuum Arc Melting	85
Table 5-7: Summary of Vacuum Induction Melting	86
Table 5-8: Summary of Heat Treat Operations	87
Table 5-9: Summary of Welding Operations	88

LIST OF FIGURES

Figure 2-1: Variation of temperature across the core during extrusion of a Ti-45.5Al-2Nb-2Cr Alloy.	2
Figure 2-2: Power-law relationship between normalized strain rate and normalized stress for cast + HIP'ed Ti-45.5Al-2Nb-2Cr alloy.	3
Figure 2-3: Effect of α grain size on flow curves of lamellar Ti-45-5Al-2Nb-2Cr alloy at 1100°C and 0.1s ⁻¹	4
Figure 2-4: Comparison of the flow curves corresponding to both isothermal and temperature transient conditions (strain rate = 1.0 s ⁻¹).	6
Figure 2-5: Schematic representation of the microstructure evolution during upsetting at 1177°C or 1093°C after preheating at 1321°C and controlled cooling.	6
Figure 2-6: (a) X-ray diffractogram obtained after heat treatment at 1200°C and (b) normalized intensities of {110} β_2 and (2021) α_2 peaks as a function of temperature.	9
Figure 2-7: Mean alpha grain size vs. heat treatment temperature.	10
Figure 2-8: Variation in the alpha grain size (D_α), gamma particle size (d_γ), and volume fraction of the gamma particles (f_γ) with annealing temperature.	12
Figure 2-9: Ratio of plane strain and uniaxial tension flow stress compared at equal levels of work rate and plastic work.	14
Figure 2-10: Failure mode map developed from simulations of the sheet tension test. The experimental results (data points) are overlaid onto the map, indicating failure control by flow localization.	15
Figure 2-11: Variation in the ductile-to-brittle transition temperature of the Ti-49.5Al-2.5Nb-1.1Mn alloy with strain rate.	17
Figure 2-12: Variation in the interlamellar spacing with the solidification rate.	20
Figure 2-13: Kinetics of the alpha growth by the peritectic reaction $L + \beta \rightarrow \alpha$	21
Figure 2-14: Time-temperature-precipitation diagram for Ti-21Al-23Nb determined from dynamic strain aging (DSA) and differential thermal analysis (DTA).	22
Figure 2-15: Flow chart showing the processing sequence for obtaining thin sheets of nickel base superalloy single crystals.	26
Figure 2-16: Predicted maximum tangential stress within the fiber as a function of degree of consolidation (fiber displacement) and preheat temperature.	29
Figure 2-17: Observations of fiber soundness in sectioned-and-polished Ti-14Al-21Nb/SCS-6 composites forge-consolidated at: (a) 1093°C and (b) 1010°C.	29
Figure 2-18: Mechanical properties of Ti-14Al-21NB/SCS-6 composites fabricated by different processing techniques.	31
Figure 2-19: Processing map for the selection of parameters to achieve full consolidation of Ti-6Al-4V/SCS-6 MMCs with optimal reaction zone thickness.	33
Figure 2-20: Dependence of the consolidation time on the strain rate sensitivity m and fixed variation in processing pressure, temperature, and fiber spacing.	34
Figure 2-21: Microstructure evolution during static recrystallization.	40
Figure 2-22: Effect of nucleation rate on static recrystallization.	40
Figure 2-23: Principle tensile stresses and plastic strain vs. distance from notch tip (a) stresses, RT, (b) stresses, -196°C, (c) plastic strain, RT, and (d) plastic strain, -196°C.	42
Figure 2-24: Heat transfer coefficient for nickel-base superalloys using the ring test.	45

FOREWORD

This report was prepared by the Materials and Processes Division of UES, Inc., Dayton, Ohio under Air Force Contract No. F33615-92-C-5900, Mr. James T. Morgan, Mr. Thomas F. Broderick and Mr. William T. O'Hara of the Materials Processing Branch of the Metals, Ceramics & Nondestructive Evaluation Division were the Government Project Engineers. The research reported herein covered the period 1 April 92 to 1 December 96.

1. Introduction

The objectives of this program were: (1) to investigate and determine the processing conditions required to achieve desired microstructures and mechanical properties in advanced aerospace materials, (2) to implement and use analytical models for process design in the Materials Processing Laboratory, (3) to validate analytical models by physical modeling, and (4) to create a center of excellence for materials processing. Primary emphasis was given to composites and high temperature materials used in advanced engines and structures.

Materials of various types and compositions were studied. In several cases, a full fledged Processing Science approach was utilized, in which the material was fully characterized in terms of microstructural and flow behavior, the proposed processing method was modeled analytically, the actual processing was carried out in the Materials Processing Laboratory (MPL) and the analytical model was validated with experimental measurements. In other cases, some of these steps were eliminated when the material or process was well understood.

2. Research on Analytical and Physical Modeling of Unit Processes

2.1 Processing of Advanced Titanium Aluminide Alloys

2.1.1 Extrusion, Forging and Rolling of Gamma TiAl

Considerable effort was devoted to develop conventional (canned) hot extrusion techniques for the breakdown of a variety of near-gamma and single-phase gamma ingot materials. The influence of can materials and geometry, can-workpiece insulation, and process variables on product integrity, yield, and the resulting microstructures were studied. Detailed finite element calculations were performed to determine the distributions of temperature, strain rate and strain. It was shown that substantial temperature nonuniformities developed during extrusion due to the complex interaction of friction, heat transfer, and deformation heating effects (Figure 2-1). Even with the use of insulation between the can and the billet, the temperature gradients were found to be sufficiently large to produce noticeable radial microstructure variations in the extrudate. Furthermore, the application of novel techniques such as controlled dwell extrusion, equal channel angular extrusion, and TMP extrusion for gamma titanium aluminides was demonstrated successfully.

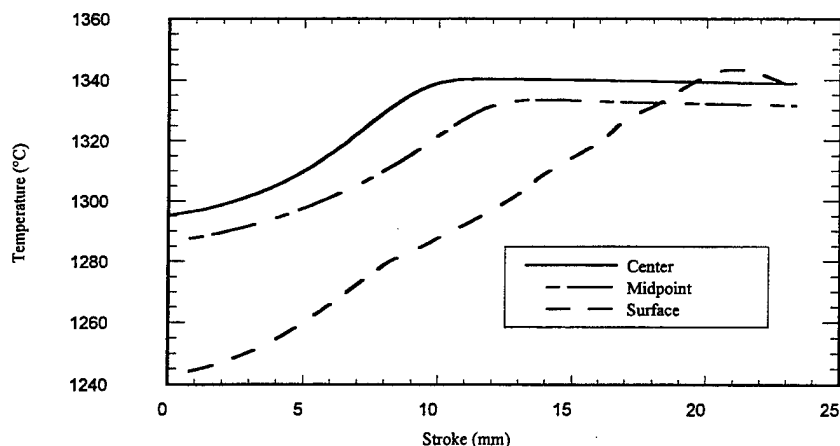


Figure 2-1: Variation of temperature across the core during extrusion of a Ti-45.5Al-2Nb-2Cr Alloy.

Isothermal forging of cast and HIP'ed billets of single-phase, as well as two-phase, gamma titanium aluminides was investigated extensively. Plastic flow behavior and microstructure development during isothermal forging were characterized using prototype forging experiments conducted at industrial forge presses as well as isothermal compression tests conducted under ideal conditions (Figure 2-2). Besides the standard isothermal forging practice which involves continuous forging at $1100^{\circ}\text{C} < T < 1175^{\circ}\text{C}$ at a constant ram velocity, several novel isothermal forging practices were developed to enhance the kinetics of globularization/recrystallization. These include two-step forging, alpha forging and smart forging.

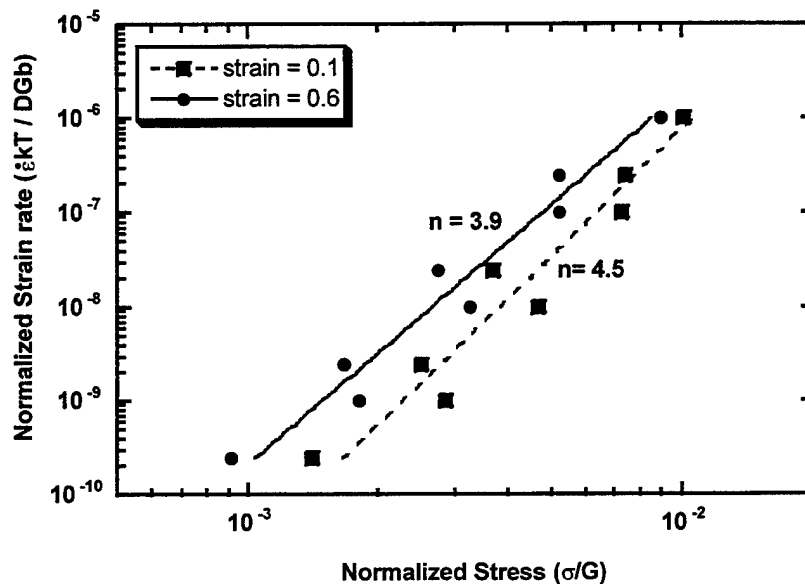


Figure 2-2: Power-law relationship between normalized strain rate and normalized stress for cast + HIP'ed Ti-45.5Al-2Nb-2Cr alloy.

The recrystallization behavior of single-phase gamma was determined via isothermal hot compression tests on Ti-49.5Al-2.5Nb-1.1Mn. The percent recrystallized structure varied in a sigmoidal fashion with strain. The logarithm of the recrystallized grain size exhibited a linear dependence on inverse temperature and inverse dependence on strain rate for deformation in the single-phase field. De-

formation at higher temperatures resulted in hot-working in the two-phase ($\alpha + \gamma$) field and thus decreasing grain size with increasing temperature due to the pinning effect of the second phase.

The influence of grain size on the kinetics of globularization of the lamellar microstructure was investigated in detail. For this purpose, fully lamellar microstructures with prior α grain sizes between $80 \mu\text{m}$ and $900 \mu\text{m}$ were developed in Ti-45.5Al-2Cr-2Nb using a special forging and heat treatment process. Isothermal compression tests were conducted at 1093°C and strain rates of 0.001 , 0.1 , and 1 s^{-1} on samples with the various grain sizes. The flow curves from these tests showed a very strong dependence of peak flow stress and flow softening rate on grain size; the larger grain-size samples exhibited significantly higher peak stresses and flow softening rates (Figure 2-3). Microstructural analysis revealed that dynamic globularization initiated at and proceeded inward from the prior- α grain boundaries. The grain interiors showed evidence of moderate-to-extensive kinking of the lamellae, depending on the orientation of the lamellae. The globularization kinetics were found to increase as the strain rate decreased, for a given α grain size, and to decrease with increasing α grain size for a given strain rate.

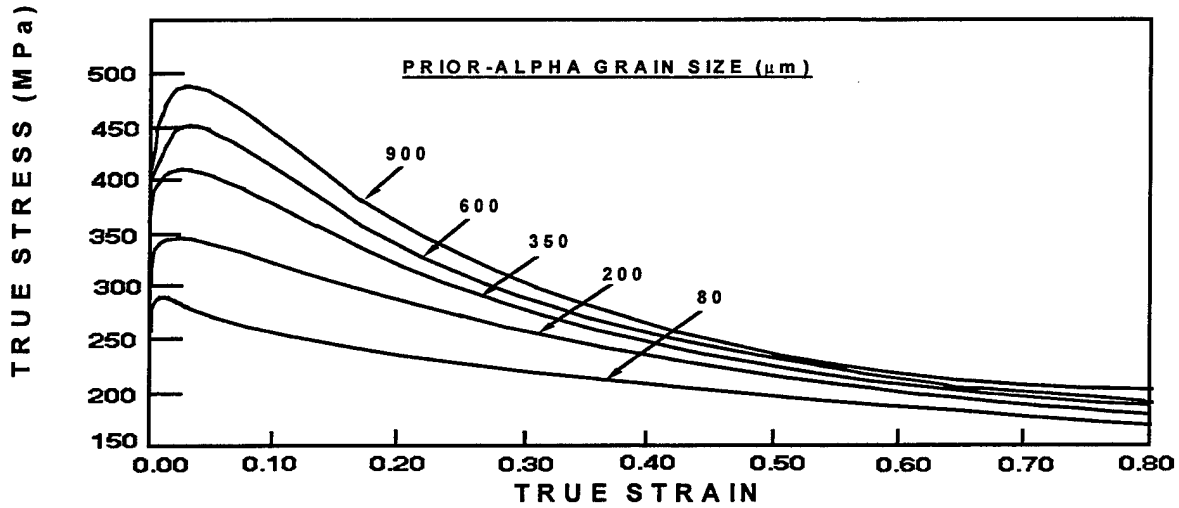


Figure 2-3: Effect of α grain size on flow curves of lamellar Ti-45.5Al-2Nb-2Cr alloy at 1100°C and 0.1s^{-1} .

Conventional hot pancake forging of cast + HIP'ed near-gamma titanium aluminide alloys such as Ti-45.5Al-2Cr-2Nb was successfully demonstrated using canned billets and cold dies. To minimize die chilling and thus the tendency for fracture, strain rates typical of conventional hot working processes ($\sim 1\text{s}^{-1}$) were used. However, even with these strain rates, the workpiece must be canned to produce a sound forging. Because of can-workpiece flow stress differences and heat transfer effects, uniform flow of can materials and gamma titanium aluminide preforms was difficult to achieve. FEM analysis showed that moderately uniform gamma pancake thicknesses can be achieved through a judicious choice of can geometry and can-workpiece insulation. Moreover, the microstructure of conventional, hot forged pancakes was found to be more uniform and finer than that obtained by isothermal forging.

Hot-pack rolling of several two-phase titanium aluminide alloys such as Ti-45.5Al-2Nb-2Cr and Ti-45.5Al-4.7Nb-1.0W, was accomplished using Ti-6Al-4V cans and preheat temperatures $\sim 40^\circ\text{C}$ to 150°C below the alpha transus. The selection of rolling parameters and pack design were aided by the development and application of analytical models which quantify the temperature transients and the stress fields during rolling. An approach based on load-signature analysis was used to verify the predictions of the above models by comparing the predicted and experimental values of the average rolling pressure. Direct heat treatments of the pack rolled sheets at subtransus as well as supertransus temperatures were used to generate a wide variety of microstructures including equiaxed, duplex, and lamellar structures. Mechanical properties of the rolled and heat treated sheets were evaluated in both the longitudinal and transverse directions.

The influence of temperature transients that occur during conventional or hot forging and pack rolling on the plastic flow behavior, fracture characteristics and microstructure evolution in a wrought Ti-45.5Al-2Nb-2Cr alloy was assessed using suitably designed hot compression experiments. Flow curves associated with supertransus preheat and subtransus upset tests exhibited very sharp peaks and

strong flow softening trends compared to those obtained under isothermal conditions, i.e., involving no temperature transients (Figure 2-4). A detailed analysis of the micromechanisms of plastic flow and structure development led to the identification of the micromechanisms of flow softening, namely the shearing/kinking and reorientation of the lamellae (texture softening) and dynamic globularization (Figure 2-5).

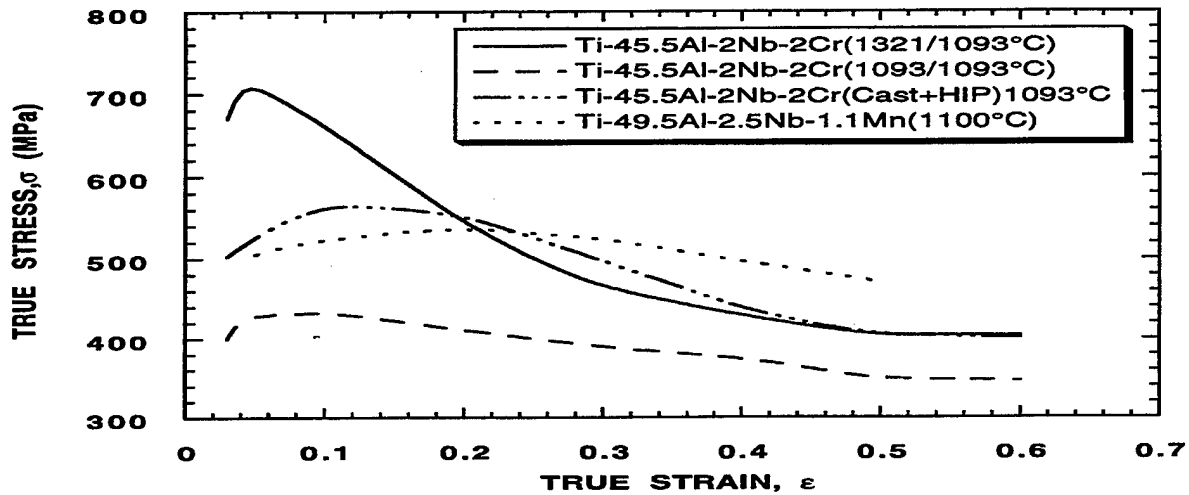


Figure 2-4: Comparison of the flow curves corresponding to both isothermal and temperature transient conditions (strain rate = 1.0 s^{-1}).

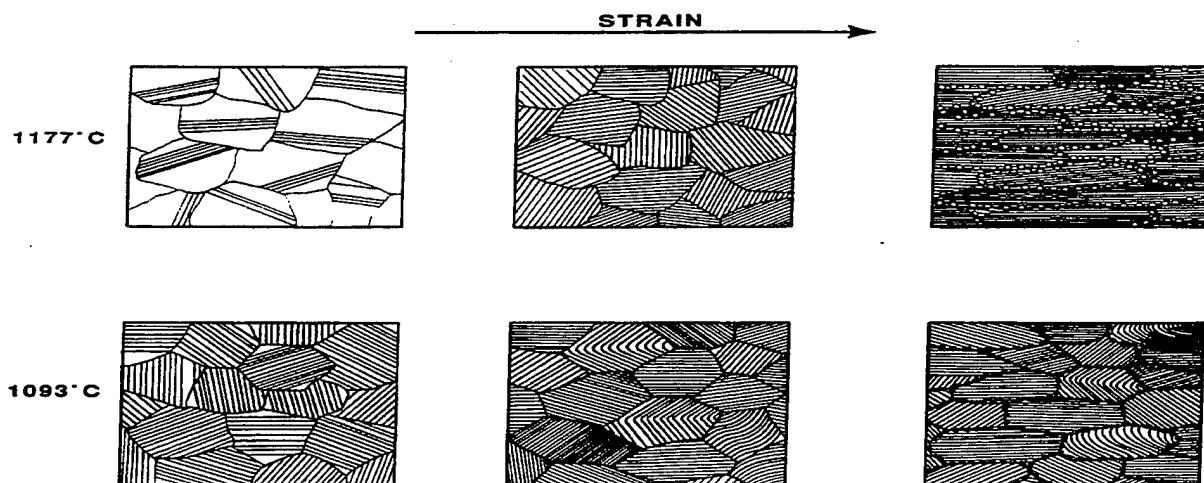


Figure 2-5: Schematic representation of the microstructure evolution during upsetting at 1177°C or 1093°C after preheating at 1321°C and controlled cooling.

Additional details regarding this work can be found in the following publications:

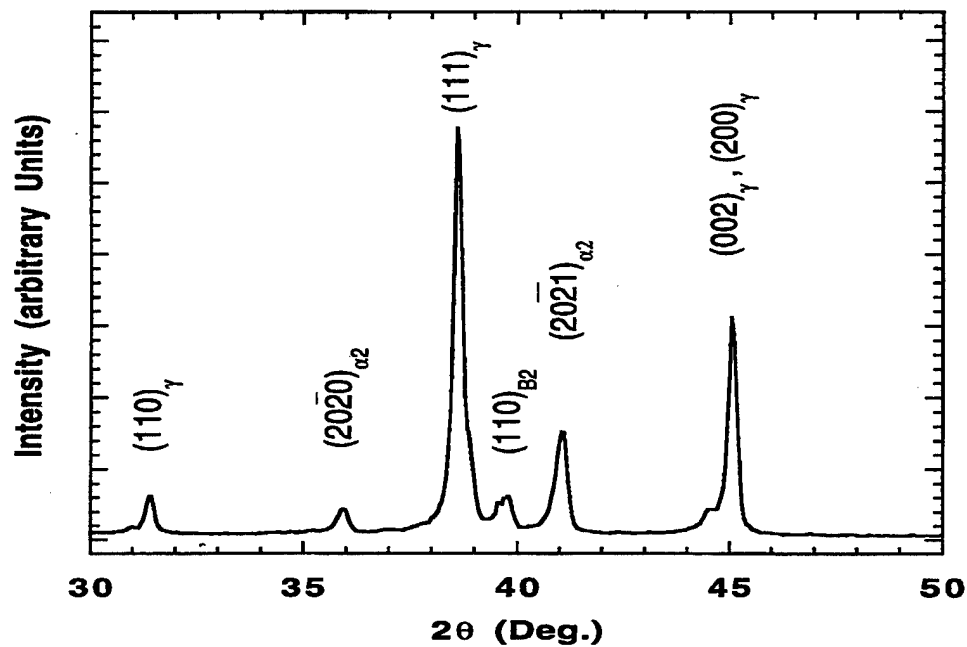
1. "Hot Extrusion of a Ti-Al-Nb-Mn Alloy", V. Seetharaman, J.C. Malas, and C.M. Lombard, High Temperature Ordered Intermetallic Alloys IV, J.O. Stiegler, L.A. Johnson, and D.P. Pope, eds., Materials Research Society, Pittsburgh, PA, p. 889 (1991).
2. "Modeling of Hot Extrusion of a Gamma TiAl Alloy", V. Seetharaman, L. Dewasurendra, A.B. Chaudhary, J.T. Morgan, and J.C. Malas, Advances in Finite Deformation Problems in Materials Processing and Structures, N. Chandra and J.N. Reddy, eds. (AMD-vol. 125), ASME, New York, NY, p. 97 (1991).
3. "Plastic Flow Behavior of a Ti-Al-Nb-Mn Alloy at High Temperatures", V. Seetharaman and C.M. Lombard, Microstructure/Property Relationships in Titanium Aluminides and Alloys, Y-W Kim and R.R. Boyer, eds., TMS, Warrendale, PA, p. 237 (1991).
4. "Effect of Core Insulations on the Quality of the Extrudate in Canned Extrusions of γ -Titanium Aluminide", R.L. Goetz, V.K. Jain, and C.M. Lombard, Journal of Materials Processing Technology, 35, pp. 37-60 (1992).
5. "Microstructure Development During Isothermal and Conventional Hot Forging of a Gamma Titanium Aluminide", S.L. Semiatin, V. Seetharaman, and V.K. Jain, Metallurgical and Materials Transactions A, Vol. 25A, p. 2753 (1994).
6. "Load-Signature Analysis for Pack Rolling of Near Gamma Titanium Aluminide Alloys", S.L. Semiatin and V. Seetharaman, Metallurgical and Materials Transactions A, Vol. 25A, p. 2539 (1994).
7. "Deformation and Microstructure Development During Hot Pack Rolling of a Near Gamma Titanium Aluminide Alloy", S.L. Semiatin and V. Seetharaman, Metallurgical and Mater. Transactions A, Vol. 26A, p. 371 (1995).

8. "Microstructures and Mechanical Properties of Rolled Sheets of a Gamma Titanium Aluminide Alloy", V. Seetharaman and S.L. Semiatin, Gamma Titanium Aluminides, Y-W. Kim, et. al., eds., TMS, Warrendale, PA, p. 753 (1995).
9. "Can Design for Nonisothermal Pancake Forging of Gamma Titanium Aluminide Alloys," V.K. Jain, R.L. Goetz, and S.L. Semiatin, Trans. ASME, J. Eng. Industry, Vol. 118, pp. 155-160 (1996).
10. "Influence of Temperature Transients on the Hot Workability of a Two-phase Gamma Titanium Aluminide Alloy", V. Seetharaman and S.L. Semiatin, Metallurgical and Materials Transactions A, Vol. 27A, pp. 1987-2004 (1996).
11. "Hot Working of Titanium Alloys—An Overview," S.L. Semiatin, V. Seetharaman, and I. Weiss, Advances in the Science and Technology of Titanium Processing, I. Weiss, et al., eds., TMS, Warrendale, PA (1996).
12. "Plastic-Flow and Microstructure Evolution During Hot Deformation of a Gamma Titanium Aluminide Alloy," V. Seetharaman and S.L. Semiatin, Metallurgical and Materials Transactions A, 28A, p. 2309 (1997).

2.1.2 Microstructure Development in Wrought Gamma Titanium Aluminide Alloys During Heat Treatments

High temperature phase equilibria in a wrought Ti-45.5Al-2Nb-Cr alloy were investigated via metallography, X-ray diffraction, and electron microprobe analysis. The alloy was extensively hot worked through a sequence of isothermal forging and pack rolling operations coupled with intermediate, recrystallization heat treatments. Specimens from the rolled sheets were subjected to prolonged isothermal heat treatments in the temperature range 900°C-1400°C for durations ranging up to 100 hours, followed by water quenching as well as slow cooling. The results indicated that a three phase equilibrium involving γ , α / α_2 , and β / β_2 phases exists in the temperature range 900°C-1250°C (Figure 2-6).

(a)



(b)

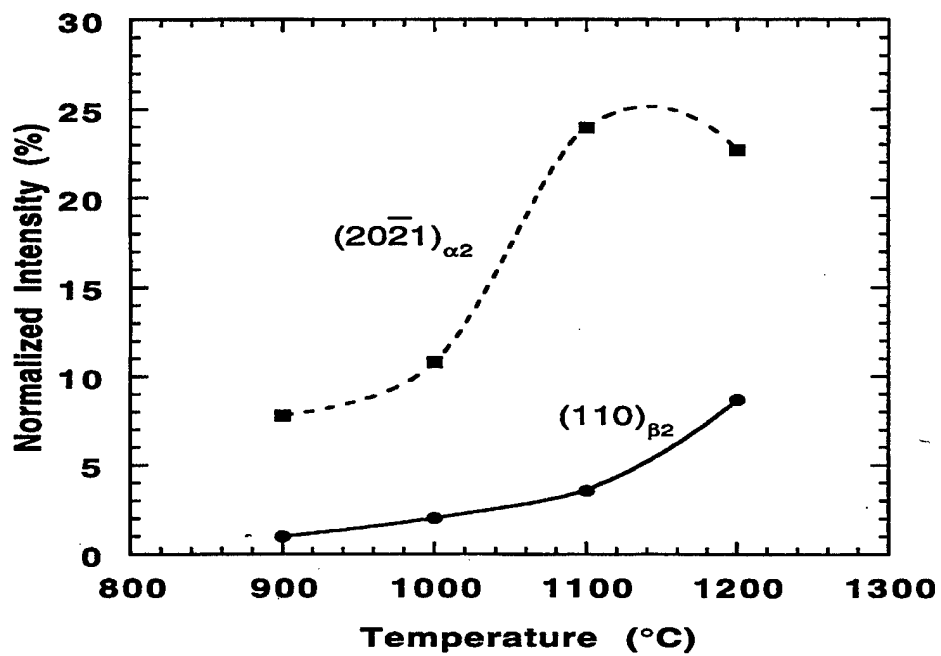


Figure 2-6: (a) X-ray diffractogram obtained after heat treatment at 1200°C and (b) normalized intensities of $\{110\}_{\beta 2}$ and $(2021)_{\alpha 2}$ peaks as a function of temperature.

While the volume fraction of β_2 appears to reach a maximum at $\sim 1200^\circ\text{C}$, that of α increases rapidly with temperature in the range 1200°C - 1300°C . Heat treatment in the single phase α field (1300°C - 1340°C) led to pronounced grain growth, whereas annealing in the $\alpha + \beta$ field ($T > 1340^\circ\text{C}$) caused retardation in the growth of α grains (Figure 2-7). The influence of heat treatment temperature and cooling rate on microstructure evolution in this alloy was analyzed in the light of available information on phase stability in Ti-Al-X systems, where X is a beta stabilizing element.

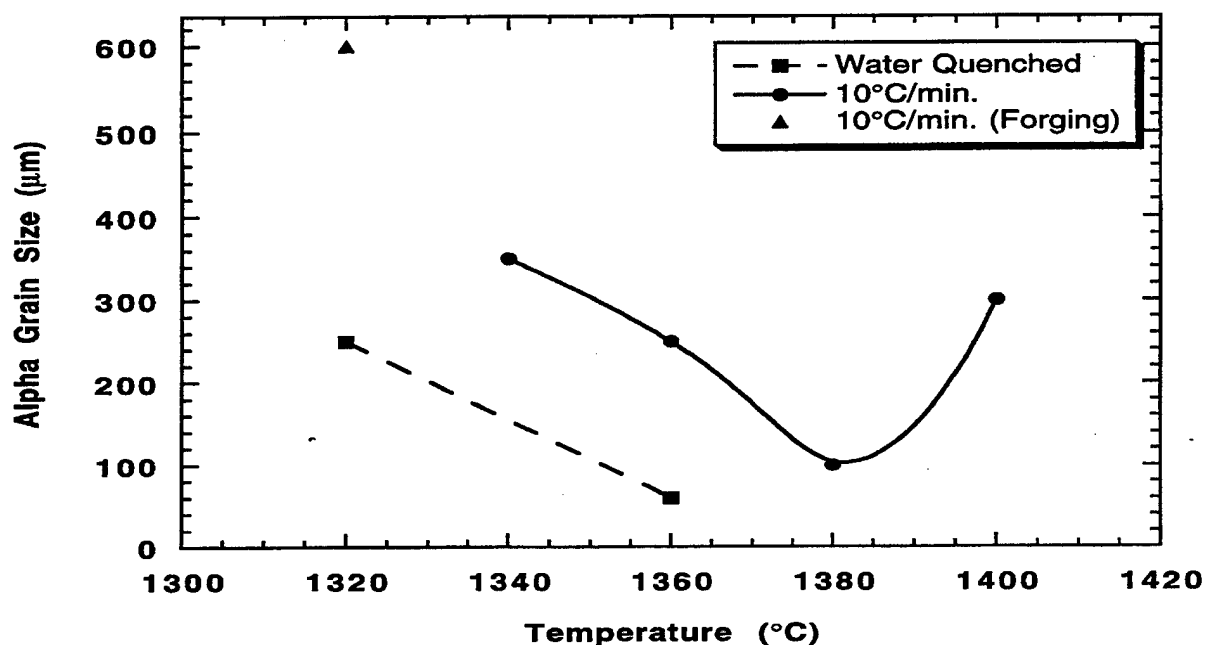


Figure 2-7: Mean alpha grain size vs. heat treatment temperature.

A companion study on the thermal processing of pack rolled Ti-45.5Al-2Nb-2Cr alloy sheets was carried out. The main goal of this investigation was to identify heat treatments which would lead to optimum tensile properties both at room temperature and at 760°C . Immediately after rolling, the packs were subjected to a variety of specially designed 'direct' heat treatments in the temperature range 1200°C - 1321°C . A variety of microstructures ranging from fine grained ($\sim 100 \mu\text{m}$) fully transformed

lamellar structure, through duplex aggregates, to a nearly equiaxed structure is observed in these sheets due to several competing transformation paths such as ordering of $\alpha \rightarrow \alpha_2$, decomposition of $\alpha \rightarrow \alpha_2 + \gamma$, and recrystallization/globularization of α/γ grains. Microduplex structures obtained in the rolled sheets were interpreted in terms of the strong temperature transients present in the final stages of pack rolling. Short term heat treatments at temperatures above the alpha transus were devised to produce fine grain (100 μm) lamellar structures.

Tensile properties and Knoop microhardness of the rolled and heat treated sheets were evaluated in both longitudinal and transverse orientations. As-rolled sheets containing fine ($\sim 3 \mu\text{m}$) gamma grains along with isolated (remnant) lamellar structures exhibited the highest tensile strength and ductility values at room temperature. Specimens heat treated at 1250°C for 20 minutes possessed a balance of tensile properties. In contrast, specimens heat treated at supertransus temperatures showed fairly high values of yield and tensile strength but relatively poor ductility. The grain size dependence of the yield strength in lamellar and duplex microstructures was interpreted in terms of the Hall-Petch relationship.

A detailed investigation of microstructure evolution in conventionally hot forged and heat treated pancakes of a Ti-45.5Al-2Nb-2Cr titanium aluminide alloy was carried out. The grain growth characteristics of the matrix alpha phase during subtransus and supertransus heat treatments were followed quantitatively. Solution annealing at temperatures above the alpha transus (1300°C) led to rapid grain growth in the alpha phase. The kinetics of alpha grain growth under these conditions conformed to a simple power-law type expression with the grain size exponent $p = 2.3$. Isochronal annealing experiments demonstrated that the volume fraction of the gamma phase, f_γ , decreases steeply with an increase in the temperature (Figure 2-8). While the mean particle size of the gamma phase, d_γ , increased gradually, the alpha grain size, D_α , increased sharply with annealing temperature, particularly above 1275°C. Isothermal annealing experiments at 1260°C revealed a slight decrease in f_γ with time. Both D_α and d_γ

increased rapidly in the early stages but approached limiting values during prolonged annealing. Experimental observations of the normalized limiting grain size of the alpha (matrix) phase (D_α/d_γ) were found to display an $f_\gamma^{-1/3}$ dependence in accordance with the model put forth by Hazzledine and Oldershaw. The kinetics of alpha grain growth at 1260°C could be analyzed with the help of a simple model based on the reduction in the driving pressure for grain growth in the alpha phase due to the drag pressure exerted by the gamma particles. A grain size exponent $p = 2.6$ was found to be appropriate for modeling the alpha grain growth at this temperature.

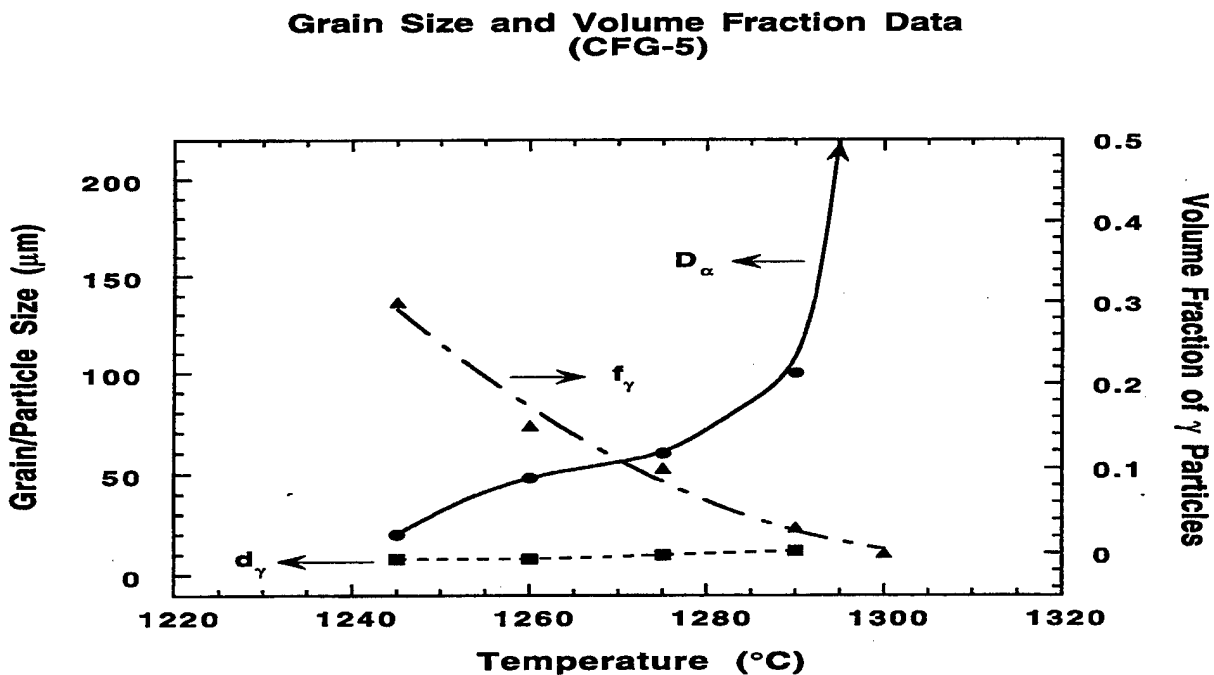


Figure 2-8: Variation in the alpha grain size (D_α), gamma particle size (d_γ), and volume fraction of the gamma particles (f_γ) with annealing temperature.

Additional details regarding this work can be found in the following publications:

1. "Deformation and Microstructure Development During Hot-Pack Rolling of a Near Gamma Titanium Aluminide Alloy", S.L. Semiatin and V. Seetharaman, Metallurgical and Materials Transactions A, 26A, p. 373 (1995).

2. "Microstructures and Mechanical Properties of Rolled Sheets of a Gamma Titanium Aluminide Alloy", V. Seetharaman and S.L. Semiatin, Gamma Titanium Aluminides, Y-W. Kim, et. al., eds., TMS, Warrendale, PA, p. 753 (1995).
3. "Microstructural Development During Conventional and Isothermal Forging of a Near Gamma Titanium Aluminide", S.L. Semiatin, V. Seetharaman and V.K. Jain, Metallurgical and Materials Transactions A, 25A, p. 2753 (1994).
4. "High Temperature Phase Stability of Ti-(45.5-48)Al-2Nb-2Cr", T. Ahmed, S. Guillard, H.J. Rack, V. Seetharaman and J.C. Chestnut, Gamma Titanium Aluminides, Y-W. Kim et. al., eds., TMS, Warrendale, PA, p. 203 (1995).
5. "Phase Stability in a Ti-45.5Al-2Nb-2Cr Alloy", V. Seetharaman, C.M. Lombard, and S.L. Semiatin, Advances in the Science and Technology of Titanium Processing, I. Weiss, et. al., eds., TMS, Warrendale, PA (1996).
6. "Analysis of Grain Growth in a Two-Phase Gamma Titanium Aluminide Alloy", V. Seetharaman and S.L. Semiatin, Metallurgical and Materials Transactions A, 28A, p. 947 (1997).

2.1.3 Deformation and Fracture of Orthorhombic Titanium Aluminide Sheets

The high temperature deformation and failure behavior of a typical orthorhombic titanium aluminide alloy (Ti-21Al-22Nb) during secondary hot working involving tensile modes of loading was established. To this end, uniaxial tension and plane-strain compression testing were conducted to determine the flow stress dependence on strain and strain rate, the level of normal plastic anisotropy, and failure modes. The results were interpreted with the aid of computer simulations based on a "direct equilibrium" model of the hot tension test.

The microstructure of the sheet comprised three phases: fine orthorhombic platelets inside an ordered beta matrix, and elongated second phase alpha-two particles. This microstructure was responsible

for the relatively low strain rate sensitivities of the material. Only at strain rates near 10^{-4} s^{-1} did m approach a value near superplastic deformation conditions (i.e., $m > 0.3$). The flow curves exhibited a peak stress at low strains followed by mild flow softening whose magnitude is greater at the higher strain rate. The flow softening was attributed to a variety of sources such as breakdown of the second phase particles and/or texture softening.

The normal anisotropy parameter was measured directly from the width and thickness strain of the deformed specimens as well as from comparison of the flow stress in tension and plane strain. The ratio of the measured plane-strain and uniaxial flow stresses ($\sigma_{\text{plane strain}} / \sigma_{\text{uniaxial}}$) were plotted as a function of plastic work (Figure 2-9). The measured data for $\sigma_{\text{plane strain}} / \sigma_{\text{uniaxial}}$ are fit best by the Hill yield function with R between 0.4 and 0.6, which is in reasonable agreement with the R value measured directly in the tension tests. Thus, to a good approximation, the Hill function can be used to model yielding behavior well at hot working temperatures.

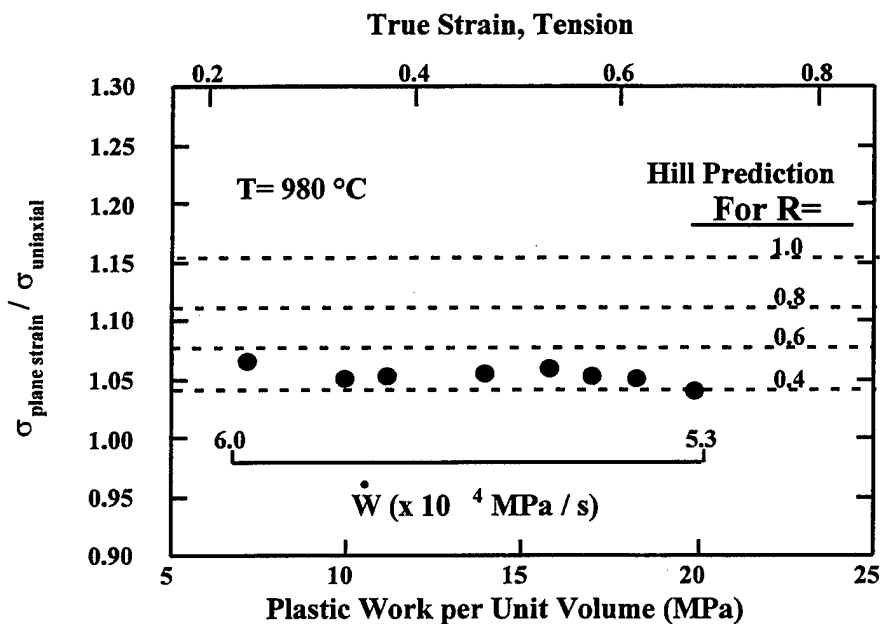


Figure 2-9: Ratio of plane strain and uniaxial tension flow stress compared at equal levels of work rate and plastic work.

The direct equilibrium approach predictions are useful in describing the competition between cavitation fracture and flow localization mode of failure, with respect to the strain rate sensitivity m , cavity growth rate η , and "initial" cavity volume fraction. Flow localization controlled failure dominates at low m and η , while cavitation failure dominates at high m and η . Figure 2-10 shows an example of such a map that displays the failure mode regimes. Experimental data from the tensile testing of the orthorhombic sheet have been also included on this map. All three data points fall into the flow localization regime, which was, in fact, the failure mode as optical microscopy revealed. This mode of failure resulted from the low strain rate sensitivities and the low cavity growth rates that the material exhibited under all of the testing conditions.

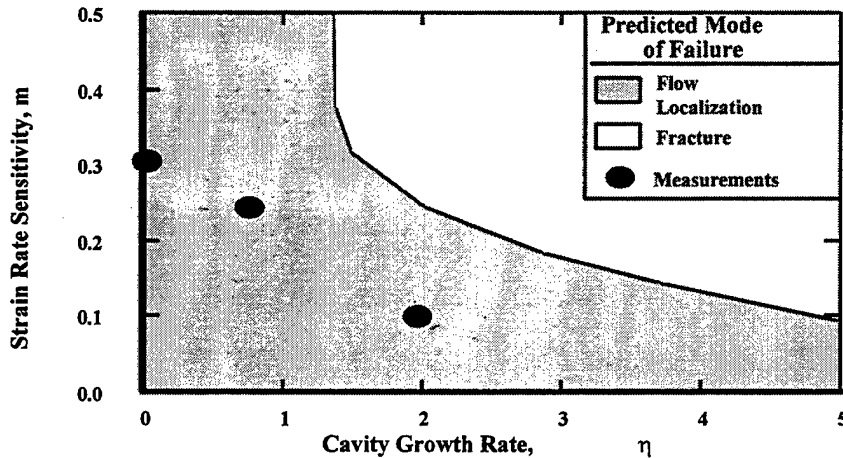


Figure 2-10: Failure mode map developed from simulations of the sheet tension test. The experimental results (data points) are overlaid onto the map, indicating failure control by flow localization.

Details of the deformation and fracture of the orthorhombic titanium aluminide sheets, and the direct equilibrium approach can be found in the following references:

1. "High Temperature Deformation of an Orthorhombic Titanium Aluminide Sheet Material", P.D. Nicolaou and S.L. Semiatin submitted to Metallurgical and Materials Transactions A, 27A, p. 3675 (1996).

2. "Simulation of the Hot Tension Test Under Cavitating Conditions", P.D. Nicolaou, S.L. Semiatin, and C.M. Lombard, Metallurgical and Materials Transactions A, 27A, p. 3112 (1996).

2.1.4 Fracture and Hot Workability of Gamma TiAl Alloys

Fracture during hot working of gamma TiAl based alloys and $\alpha + \beta$ titanium alloys occurs in two distinct regimes: (i) brittle, intergranular failure induced by wedge cracking occurring at low temperatures and high strain rates, and (ii) ductile fracture caused by nucleation, growth and coalescence of cavities occurring at high temperatures and relatively low strain rates. In order to characterize both these types of fractures, tension tests were conducted on a Ti-49.5Al-2.5Nb-1.1Mn alloy in cast and wrought, conditions, over a wide range of temperatures and strain rates. For both conditions, a transition from brittle to ductile behavior was observed over a narrow temperature range. The transition temperature increased with an increase in strain rate. Furthermore, the transition temperatures for a given strain rate were higher for the coarse-grained cast material than for the finer grained, wrought material (Figure 2-11). An Arrhenius-type analysis of the transition temperature vs. strain rate data showed that the transition from brittle to ductile fracture is controlled by the onset of dynamic recrystallization. Tension tests conducted on a wrought Ti-45.5Al-2Nb-2Cr alloy also confirmed the importance of both applied stress and the scale of microstructural features in controlling wedge cracking. Intergranular cracking and fracture were modeled by assuming that cracks form by the linkage of ventricular voids nucleated at the intersection of shear bands and grain boundaries, by the combined action of grain boundary sliding and pile-up stresses. Accordingly, a grain-size dependent critical stress for the onset of intergranular fracture was derived. Using constitutive equations for plastic flow, processing maps delineating brittle and ductile fracture regimes in the temperature-strain rate space were constructed. Critical stress vs. grain size data were also interpreted in terms of a Griffith-type criterion based on a critical stress intensity factor.

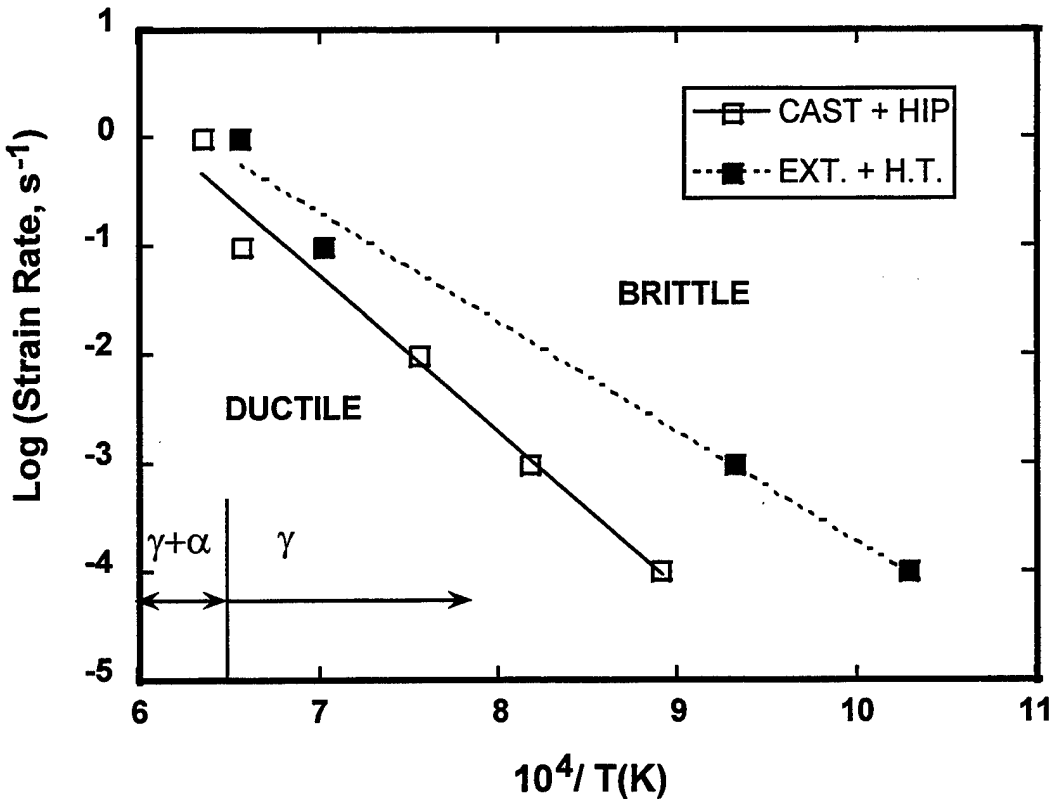


Figure 2-11: Variation in the ductile-to-brittle transition temperature of the Ti-49.5Al-2.5Nb-1.1Mn alloy with strain rate.

Free surface cracking of Ti-49.5Al-2.5Nb-1.1Mn during pancake forging due to secondary tensile stresses was analyzed in detail. The critical conditions required for the onset of free surface cracking were predicted using the maximum tensile work criterion proposed by Cockroft and Latham. This approach was successful in explaining the influence of temperature, strain rate, and die-workpiece friction on the incidence of cracking. Furthermore, the effect of superimposed hydrostatic pressure on the hot workability of the above alloy was investigated. While there was no noticeable effect of pressure on flow stress and the dynamic recrystallization process, both free surface cracking and sub-surface void formation were suppressed entirely under superimposed hydrostatic pressure. It was demonstrated that

the magnitude of the hydrostatic pressure required to overcome the free surface cracking is approximately one-half of the effective stress.

Additional details regarding this work can be found in the following publications:

1. "Tensile Fracture Behavior of a Cast Gamma Titanium Aluminide", V. Seetharaman, R.L. Goetz, and S.L. Semiatin, High Temperature Ordered Intermetallic Alloys IV, J.O. Stiegler, L.A. Johnson, and D.P. Pope, eds., Materials Research Society, Pittsburgh, PA, p. 895 (1991).
2. "Effect of Hydrostatic Pressure on the Hot Working Behavior of a Gamma Titanium Aluminide", D. Watkins, H.R. Piehler, V. Seetharaman, C.M. Lombard, and S.L. Semiatin, Metall. Trans. A, Vol. 23A, p. 2669 (1992).
3. "Deformation and Fracture Characteristics of a Gamma Titanium Aluminide at High Temperatures", V. Seetharaman, S.L. Semiatin, C.M. Lombard, and N.D. Frey, High Temperature Ordered Intermetallic Alloys V, I. Baker, R. Darolia, J.D. Whittenberger, and M.H. Yoo, eds., Materials Research Society, Pittsburgh, PA, p. 513 (1993).
4. "Intergranular Fracture of Gamma Titanium Aluminides under Hot Working Conditions", V. Seetharaman and S.L. Semiatin, Metallurgical and Materials Transactions A (submitted).
5. "A Criteria for Intergranular Failure During Hot Working of Near Gamma Titanium Aluminide Alloy", S.L. Semiatin and V. Seetharaman, Scripta Mater, Vol. 36, p. 291 (1997).
6. "Plastic Flow and Microstructure Evolution during Hot Deformation of a Gamma Titanium Aluminide Alloy", V. Seetharaman and S.L. Semiatin, Metallurgical and Materials Transactions A, 28A, p. 2309 (1997).

2.1.5 Directional Solidification of a Ti-48Al-2Nb-2Cr Alloy

As part of the Processing Science Program conducted by the General Electric Company under contract F33615-C-91-5648, a focused research activity on the directional solidification (D.S.) of a Ti-

48Al-2Nb-2Cr Alloy was undertaken by UES. This study involved theoretical analysis of the peritectic solidification as well as experimental work carried out using a D.S. apparatus available at the University of Cincinnati. Cylindrical rods of approximately 10 mm diameter machined from a cast and HIP'ed ingot of the Ti-48Al-2Nb-2Cr alloy were used for this investigation. The D.S. apparatus consisted of a high vacuum system, radio frequency induction heater with a graphite susceptor, and a water cooled chill plate which could be withdrawn at a controlled velocity. The specimens were melted in argon atmosphere inside an alumina tube. The bottom end of the tube was cooled indirectly by the chill plate. Directional solidification was achieved by withdrawing the alumina tube containing the molten alloy through the chill plate at a constant velocity. A constant temperature gradient of $\sim 16.5 \text{ }^\circ\text{C mm}^{-1}$ at the solid-liquid interface was maintained for all the experiments. Several D.S. runs were made with the solidification rate varying from 10 to $200 \text{ } \mu\text{m s}^{-1}$. Detailed microstructural studies including scanning electron microscopy and electron microprobe analysis were carried out on the longitudinal sections of the solidified rods.

As a result of interactions between the alumina tube and molten titanium aluminide, Al_2O_3 particles were found to be dispersed throughout the solidified alloy. The volume fraction, size, and morphology of the Al_2O_3 particles varied with the solidification rate. The presence of the Al_2O_3 particles did not, however, affect the solidification behavior of the alloy. Microstructures of the D.S. alloy in general consisted of columnar arrays of (prior) alpha grains containing $\gamma + \alpha_2$ lamellae. The interlamellar spacing was found to decrease systematically with the solidification rate. Figure 2-12 compares the spacing vs. solidification rate data obtained in the current work with the results obtained by Takeyama and his coworkers.

In gamma titanium aluminide alloys containing Al - 47 at.% and significant additions of Nb, Ta, V, and Cr, β is the primary phase to nucleate during solidification at low rates. Following the crystalli-

zation of β , two successive peritectic reactions occur, producing α and γ phases, respectively. However, it is often difficult to determine experimentally the extent to which these reactions proceed. Accordingly, the kinetics of these reactions/transformations were studied analytically. A simple model for peritectic transformations dealing with the kinetics of diffusion-controlled thickening of the peritectic envelope was developed. Using this model, the rates of the two transformations mentioned above were calculated.

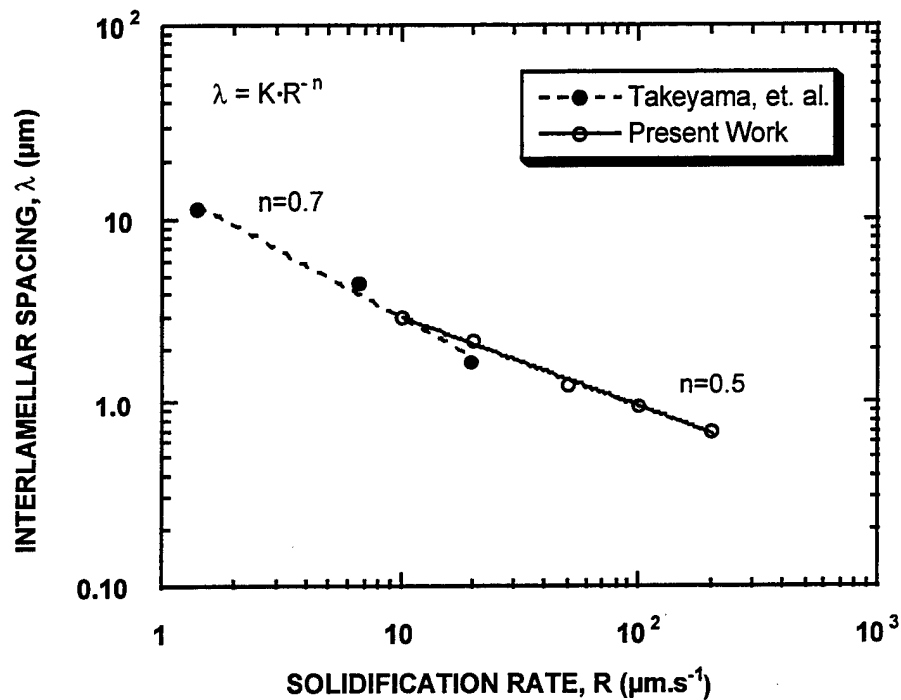


Figure 2-12: Variation in the interlamellar spacing with the solidification rate.

Figure 2-13 illustrates the dominant influence of undercooling on the growth (thickening) rate of α formed at the interface between the liquid and the β phase. Considering the effects both time and temperature on growth rate, an average growth rate of α in the temperature interval of about 35°C between the two peritectic reactions was estimated as approximately 1 $\mu\text{m/s}$. In contrast, the average growth rate for the second peritectic reaction ($L + \alpha \rightarrow \gamma$) was calculated to be at least three orders of magnitude

lower than that of the first reaction. These results are consistent with the experimental findings that even at relatively low solidification rates (e.g., 10 $\mu\text{m/s}$), no evidence for the formation of peritectic γ phase could be found.

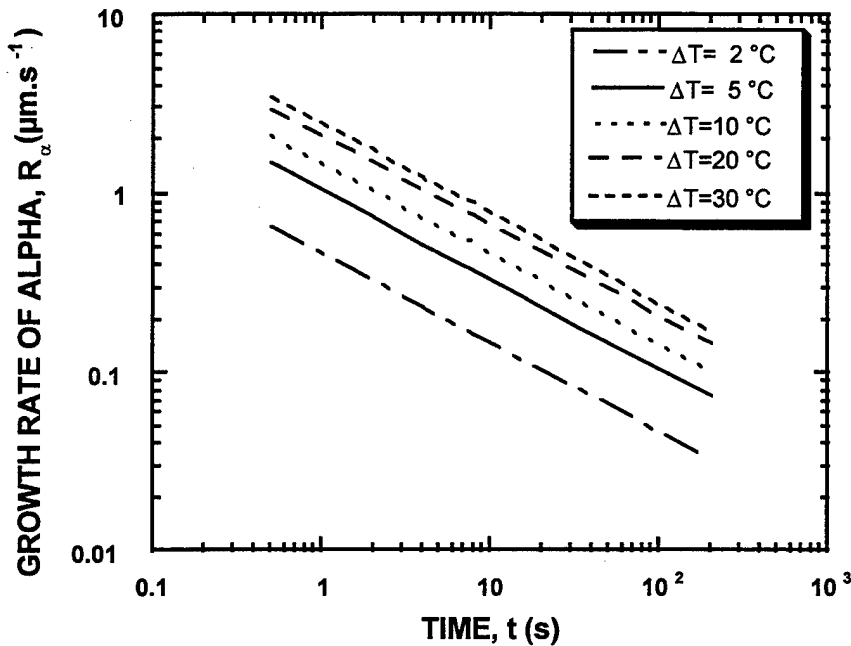


Figure 2-13: Kinetics of the alpha growth by the peritectic reaction $L + \beta \rightarrow \alpha$.

2.1.6 Plastic Flow and Phase Stability in Orthorhombic Alloys

A hot workability study was conducted on an orthorhombic Ti-21Al-23Nb alloy using isothermal, constant velocity compression tests, over the temperature range 900°C to 1155°C and the nominal strain rate range 0.001 to 1.0 s^{-1} . Three different microstructures corresponding to (a) hot rolled and mill annealed, (b) β_0 -heat treated, and (c) β_0 solution treated and direct aged conditions were examined. These microstructures varied from a relatively coarse distribution of O-phase precipitates in a matrix of transformed β_0 to the metastable retained β_0 . Flow stress displayed a sharp dependence on temperature, strain rate and on the initial structure. While uniform plastic flow was obtained at high temperatures and for structures containing primary O, β_0 -heat treated structures led to pronounced flow soften-

ing. Intense shearing and kinking of the fine, O-phase needles present in the transformed β_0 led to flow softening. Strong yield point phenomena and serrated flow were observed in selected test conditions and for microstructures containing high volume fractions of metastable β_0 . These flow instabilities resulting from Luder band propagation and dynamic strain aging were interpreted in terms of dislocation-solute interactions in supersaturated β_0 . Plastic flow behavior of solution treated and direct aged specimens revealed interesting transitions from serrated, work hardening type of flow curves at short aging times to smooth, flow softening type of flow curves at long aging times (Figure 2-14). These results suggest that the depletion of aluminum and enrichment of niobium in β_0 caused by the precipitation of O-phase were responsible for the transition from serrated to smooth plastic flow. This confirmed the conclusion that solute-dislocation interactions in supersaturated β_0 cause serrate flow. In a parallel effort, phase transformations occurring in Ti-21Al-23Nb alloy during continuous heating/cooling experiments were studied by DTA and dilatometry methods. Activation energy for the precipitation of the O-phase was determined as 263 kJ/mol and was approximately equal to that for diffusion of Nb in highly alloyed β/β_0 phase of titanium.

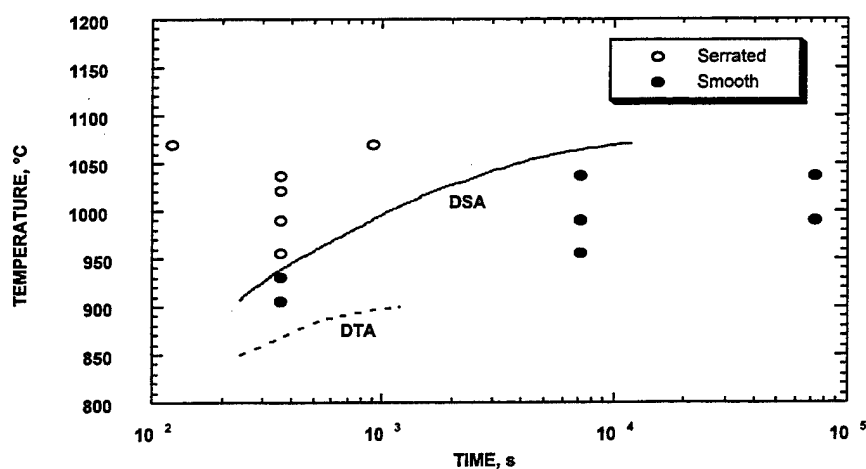


Figure 2-14: Time-temperature-precipitation diagram for Ti-21Al-23Nb determined from dynamic strain aging (DSA) and differential thermal analysis (DTA).

Tensile and creep behavior of a new orthorhombic alloy, Ti-25Al-25Nb, was investigated as a function of processing and microstructure. Thermomechanical processing techniques comprising nonisothermal forging and pack rolling were used to obtain 2 mm thick sheets. A variety of microstructures were achieved through post-processing heat treatments. The microstructures consisted of a mixture of β_2 and O, with the amount of β_2 ranging from 0 to 60 percent. All creep experiments were performed in air at 650°C and 172 MPa. Supertransus ($T > T_B \sim 1000^\circ\text{C}$) processed sheets suffered from intergranular attack and exhibited low ductility. Subtransus processing and heat treatment resulted in the best combination of room and elevated temperature properties. While the microstructure containing the highest volume fraction of β_2 exhibited the poorest creep performance, it was associated with the highest values of tensile strength and elongation at room temperature. In contrast, equiaxed, fully orthorhombic microstructures exhibited excellent creep resistance, but suffered from low strain-to-failure ($< 1\%$) due to intergranular cracking. On the other hand, microstructures in which a continuous layer of β_2 was sandwiched between adjacent O grains, yield tensile elongations up to 5 percent. This improvement in ductility was attributed to extensive slip interaction occurring between orthorhombic and β_2 grains. Furthermore, lath microstructures exhibited significant improvement in creep performance compared to equiaxed microstructures containing approximately the same volume fractions of O and β_2 . Microstructural effects on tensile properties, steady state creep behavior, and damage accumulation were analyzed in the light of existing models on plastic deformation of two-phase materials.

Additional details of this work are found in the following references:

1. "Deformation Behavior of an O + β_O Processed Ti-21Al-23Nb Alloy at High Temperatures", V. Seetharaman, High Temperature Ordered Intermetallic Alloys VI, J.O. Horton, et al., eds., Materials Research Society, Pittsburgh, PA, Vol. 364, p. 1253 (1995).

2. "Processing and Heat Treatment Effects on the Phase Evolution and on the Tensile and Creep Behavior of a Ti-25Al-25Nb Alloy", C.J. Boehlert, B.S. Majumdar, V. Seetharaman, and D.B. Miracle, Deformation and Fracture of Ordered Intermetallics, W-O. Soboyejo, et al., eds., TMS, Warrendale, PA (in press).

2.2 Pack Rolling of Single Crystal Nickel Base Superalloys

Thin sheets (~ 0.50 mm) of single crystal nickel base superalloys are required for use in some critical components of the F-22 aircraft system. These components demand high stiffness, tensile and creep strength and high cycle fatigue properties at elevated temperatures approaching 1000°C. Single crystal superalloys such as PWA 1480 and its successors are good candidate materials capable of satisfying the preceding requirements. Two possible routes for fabrication of thin sheets are: (i) production of ultra-thin sheet castings, and (ii) casting of thick plates and hot working of the plates to thin sheets. Since the direct casting approach is fraught with major difficulties such as incomplete die fill, cold sheet, shrinkage porosity, etc., the latter approach was taken up for a detailed study.

The main drawback of the deformation processing approach is the possible occurrence of dynamic/static recrystallization of the alloy during multipass deformation/heating cycles. Moreover, single crystal superalloys contain typically 40-60 percent of the strengthening phase, γ' and were designed primarily as cast alloys. These alloys are, therefore, not very amenable for hot working. Processing windows are generally very narrow and special procedures have to be devised to avoid fracture and cracking during hot working. One approach to reduce the deformation resistance of γ' strengthened superalloys is to effectively increase the γ' particle size without altering its volume fraction. It is possible to overage the γ' particles (at constant volume fraction) by heating the alloy and soaking at temperatures just below the γ' solvus and cooling the alloy very gradually through the γ' precipitation regime. This technique prevents additional nucleation of γ' particles and enables the growth of the particles existing at the soaking temperature.

A major scientific objective of this program was to identify and control multipass, pack rolling conditions for cast single crystal nickel base superalloys, which will permit significant thickness reductions without (a) concomitant dynamic/static recrystallization, and (b) intervention of cracking/fracture. Dynamic recrystallization can occur during a rolling pass if the reduction per pass exceeds a critical strain, ϵ_c the magnitude of which depends on the rolling speed and temperature. Thus the occurrence of dynamic recrystallization during rolling can be avoided by selecting temperatures and strain rates such that the strain corresponding to each pass does not exceed ϵ_c . Static recrystallization occurs during reheating between successive rolling passes. The kinetics of this process are very complex and depend on several variables. In general, the extent of static recrystallization increases with reheat temperature and time; it also depends on the reduction during the previous pass and the cumulative reduction up to that stage. Fracture during rolling can be avoided if narrow temperature windows below the γ' solvus can be selected and if the strain rate during rolling is not excessively high. Temperature control of the workpiece is accomplished through the use of pack rolling procedures involving suitable cover plates, metal/insulator layers.

The program consisted of developing the complete processing sequence for converting thick slabs of superalloy single crystal castings into 0.5 mm thick sheets/foils. The flow chart shown in Figure 2-15 summarizes the different operations and the sequence in which they were carried out for achieving the final product. Cast single crystal bars grown along specific crystallographic directions, viz., [001] were subjected to prolonged overaging heat treatments in vacuum. Typically, these treatments consisted of isothermal holding at 1270°C for 1 hour, cooling at the rate of 5°C per hour in the temperature range 1270°C to 1035°C, 30°C per hour in the temperature range 1035°C to 815°C, and 5°C per minute at temperatures below 815°C. The microstructure of the overaged alloy consisted of coarse γ' particles with a mean size of $\sim 5 \mu\text{m}$. The workpiece was packed inside stainless steel or Hastelloy-X cover sheets along

with refractory metal interlayers and insulating coatings at the internal surfaces. After evacuation and sealing, the packs were preheated at 1100°C to 1150°C for 1 hour and rolled through a series of passes. The reduction per pass was ~ 10%, and the total reduction in thickness per campaign was within 50-75 percent. After rolling the pack was decanned and the rolled sheet was reconditioned, repacked and rolled again until the final goal of 0.5 mm thickness was achieved. Metallographic and x-ray diffraction analysis of the sheets confirmed the single crystalline nature of the product.

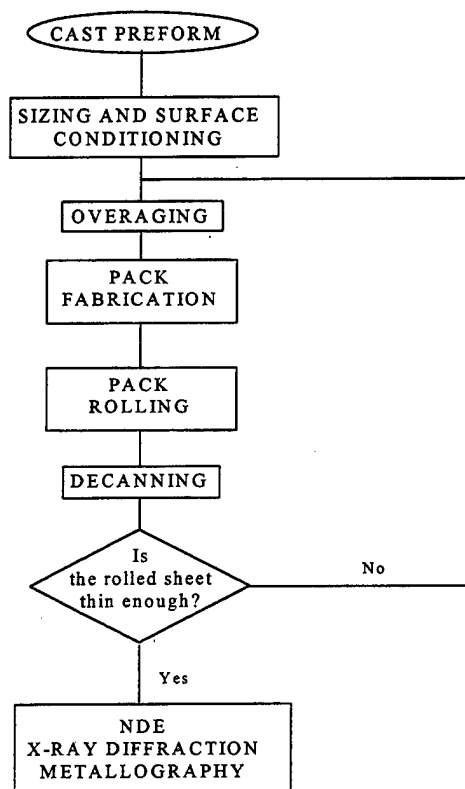


Figure 2-15: Flow chart showing the processing sequence for obtaining thin sheets of nickel base superalloy single crystals.

Additional details of this work can be found in the following invention disclosure:

1. "Method for Hot Rolling Single Crystal Nickel Base Superalloys" V. Seetharaman, S.L. Semiatin, and C.A. Lombard, Air Force Invention Disclosure, 1994.

2.3 Rapid Consolidation of Continuously Reinforced MMCs

The feasibility of the rapid consolidation of Ti-14Al-21Nb/SCS-6 foil/fiber/foil composites using a forging approach was established as an alternative to slower, and therefore, more expensive processes such as those based on hot isostatic or vacuum hot pressing. A firm basis for the technique was developed through theoretical and experimental analyses of temperature transients, forging speeds, fiber fracture, composite macrostructure and microstructure. In addition, the quality of the forge-consolidated articles was examined by conducting room temperature tensile and fatigue testing.

A lumped-parameter heat transfer model was developed to quantify the temperature transient behavior. The temperature versus time profile of the foils and the encapsulation was established. The analysis revealed that substantial temperature transients occur during the forge consolidation process. The most significant and pronounced temperature drop occurs during the forging period, because the applied consolidation pressure gives rise to much higher interface heat transfer coefficients between the dies and the workpiece.

The temperature transient results were used to estimate an optimal forging speed, i.e., the speed at which the forging load (and hence the loads imposed on the fibers) is a minimum. A high forging speed leads to a higher matrix strain rate, and therefore, larger consolidation loads. On the other hand, at higher forging speeds, heat losses are lower, temperatures are higher, and therefore, the required loads are smaller. The combination of those two opposing effects led to the determination of the optimum forging speed.

Three possible sources of fiber fracture during forge consolidation of foil/fiber/foil lay-ups may be hypothesized. These are the following:

1. Radial cracking due to tensile tangential stresses in the SiC sheath. These stresses arise in the SiC layer because the carbon core is much more compliant than its surrounding silicon carbide.
2. Axial fracture due to axial tensile stresses generated in the fibers. Axial tensile stresses are developed to balance the transverse compressive stresses in the matrix foils, which deform under plane strain conditions during forge consolidation
3. Fracture due to fiber bending induced by the crossweave wires. This mode of fracture was avoided by minimizing the fiber bending stresses, by replacing the crossweave wires with thin ribbons and maximizing the distance between the ribbons in alternating fiber mats.

With respect to the first possible mechanism, Figure 2-16 shows FEM predictions of the maximum tangential stress in the SiC layer versus fiber displacement (or equivalently degree of consolidation) for four different preheat temperatures. The transverse strength of the SCS-6 fiber is also plotted in Figure 2-16. It reveals that preheat temperatures below 1050°C should be avoided because the required loads cause the maximum tensile stress in the SiC to be larger than its tensile strength. On the other hand, the results indicate that preheat temperatures close to 1100°C should enable the forge consolidation of composites without significant fiber damage. Experimental observations agreed well with the above predictions. Figure 2-17(a) shows a micrograph of a composite forge consolidated at 1093°C. No radial cracks in the fibers were observed. On the other hand, for lay-ups forged after preheating at 1010°C, the fibers suffered extensive radial cracking, Figure 2-17(b).

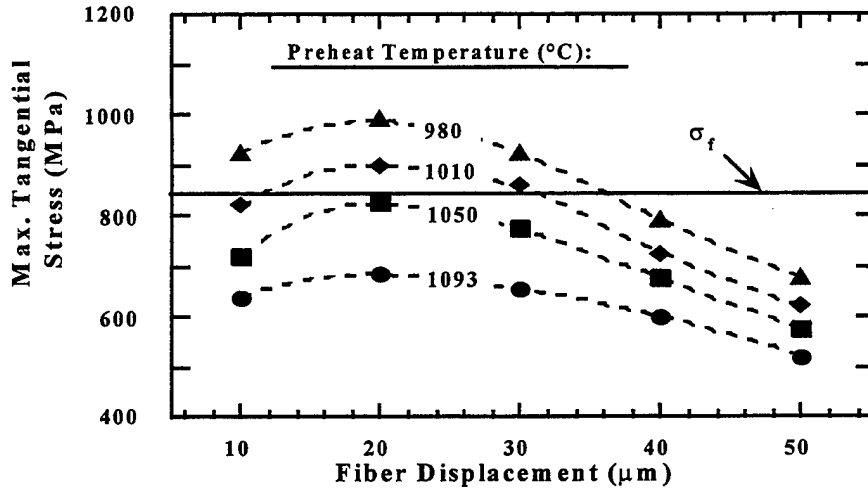


Figure 2-16: Predicted maximum tangential stress within the fiber as a function of degree of consolidation (fiber displacement) and preheat temperature.

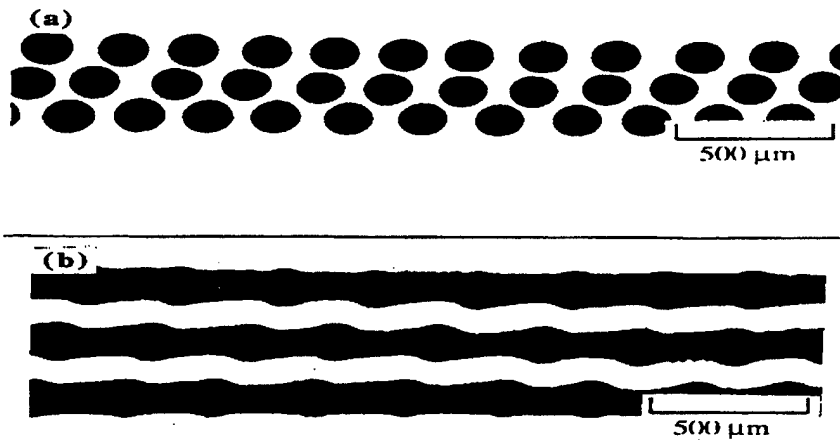


Figure 2-17: Observations of fiber soundness in sectioned-and-polished Ti-14Al-21Nb/SCS-6 composites forge-consolidated at: (a) 1093°C and (b) 1010°C.

With regard to the axial mode of fracture, an analysis of estimating the axial stresses was performed. The results reveal that tensile stresses less than one-fifth of the tensile strength of the fiber are generated. Thus, fiber fracture by this mechanism is not expected, nor was it observed. In particular, forge-consolidated samples of Ti-14Al-21Nb/SCS-6 were etched to remove the matrix. It was found that 95 percent of the fibers had lengths equal to or greater than 0.9 times the nominal composite length.

With regard to the composite macrostructure, it was found that the flow stress of the encapsulation material is important to ensure the closure of porosity. Theoretical analysis revealed that a higher flowstress encapsulation material is required in order to minimize the secondary in-plane tensile stresses and close any remnant porosity. These predictions were experimentally validated by examining the level of consolidation achieved in composites encapsulated in mild and stainless steel cans. Examination of the composite microstructure showed that there is a tendency for localization of plastic flow. However, a rapid post-consolidation heat treatment was developed; a uniform, fully recrystallized microstructure, similar to that of conventional (slow) processes was produced.

Room temperature tensile and fatigue testing was performed in order to assess the quality of the forge-consolidated MMCs. From the tensile tests, the elastic modulus, ultimate tensile strength, and strain to failure were determined and compared to the properties determined on foil/fiber/foil, powder-cloth, and plasma-spray monotape lay-ups, of the same unidirectional fiber architecture, that had been HIP consolidated (Figure 2-18). Inspection of the results reveals that overall the tensile properties of the forge-consolidation Ti-14Al-21Nb/SCS-6 composites are quite comparable to those of conventionally-processed ones. Similarly, the fatigue results in terms of cycles to failure versus maximum applied stress, or strain range demonstrated that no-property loss occurred during the faster, however, lower cost forge consolidation method.

Details of the rapid consolidation of MMCs can be found in the following references:

1. "An Experimental and Theoretical Investigation of the Rapid Consolidation of Continuously-Reinforced, Metal-Matrix Composites", P.D. Nicolaou, S.L. Semiatin, and R.L. Goetz, Metallurgical and Materials Transactions A, 27A, p. 1719 (1996).

2. "Fiber Fracture During the Processing of Continuous Fiber Metal-Matrix Composites Using the Foil/Fiber/Foil Technique", P.D. Nicolaou, H.R. Piehler, and S.L. Semiatin, Metallurgical Mater. Trans. A, 26A, No. 5, pp. 1129-1140 (1995).
3. "Processing and Properties of Rapidly-Consolidated Metal Matrix Composites", P.D. Nicolaou and S.L. Semiatin, Processing of Advanced Materials IV, T.S. Srivatsan and J.J. Moore eds., The Minerals, Metals, and Materials Society, Warrendale, PA, 1996, pp. 547-560.

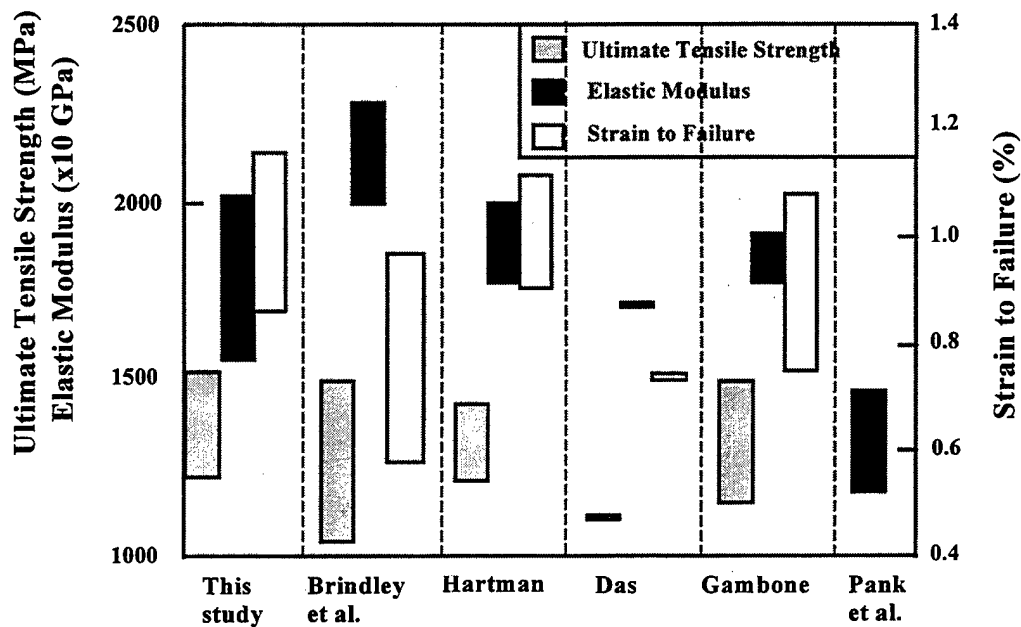


Figure 2-18: Mechanical properties of Ti-14Al-21Nb/SCS-6 composites fabricated by different processing techniques.

2.4 Design of Consolidation Practices from Foil/Fiber/Foil Lay-ups

Process Parameter Selection: A methodology for the selection of the processing parameters for consolidation of foil/fiber/foil lay-ups, such as defects or other irregularities (i.e., extensive fiber-matrix interfacial reactions, residual porosity, fiber fracture, etc.) in the finished product are avoided, was estab-

lished. Specifically, for consolidation of a specific composite system the following issues have to be addressed when selecting the processing parameters:

- fiber-matrix interfacial reactions, which depend on the temperature and processing time.
- consolidation kinetics, which depend on the applied pressure, temperature, lay-up geometry, and fiber volume fraction.
- fiber fracture, which depends upon the lay-up geometry, applied pressure, temperature, and fiber volume fraction.

In addition, there are usually equipment, material, and process economics limitations, that impose further constraints on the selection of pressure, temperature, and time.

Analytical derivation of a suitable processing window satisfying the above constraints, by combining previously derived closed form equations which correlate the above issues to the processing parameters, is extremely difficult because of the complex form of the analytical expressions. To this end, an example of the application of the methodology was illustrated using a graphical approach for a specific MMC system consisting of a Ti-6Al-4V matrix and SCS-6 silicon carbide fibers (Figure 2-19). Combinations of temperature and time in the shaded region of Figure 2-19 result in composites with desirable reaction zone subject to the constraints of T_{\max} and t_{\max} . The intersection of the constant-pressure, consolidation curves with the shaded region, thus, defines the acceptable processing regime for the chosen lay-up geometry.

Sensitivity Analysis: The sensitivity of the consolidation time for foil/fiber/foil lay-ups to lot-to-lot matrix flow stress variations, as well as variations of temperature, pressure and fiber spacing was also established. It was found that lot-to-lot variations in the flow stress-strain rate behavior for the alpha-two titanium aluminide alloy Ti-14Al-21Nb may give rise to required consolidation times which vary approximately by a factor of 6. Much smaller variations in material behavior and, hence, consoli-

dation time were predicted for the conventional titanium alloy Ti-6Al-4V. With regard to the sensitivity of the consolidation time to variations on pressure, temperature, and fiber spacing, the results are shown in Figure 2-20. The dependence of $\delta t_c/t_c$ on the value of the strain rate sensitivity m for a 50K temperature variation, a 10 percent pressure variation, or a 20 μm variation in fiber spacing is summarized in Figure 2-20. The results in this plot revealed a very strong dependence of $\delta t_c/t_c$ on m . From such a behavior, it was concluded that high values of m are desirable with regard to designing a reproducible, robust consolidation cycle, something that was also considered in selecting processing temperatures and pressures.

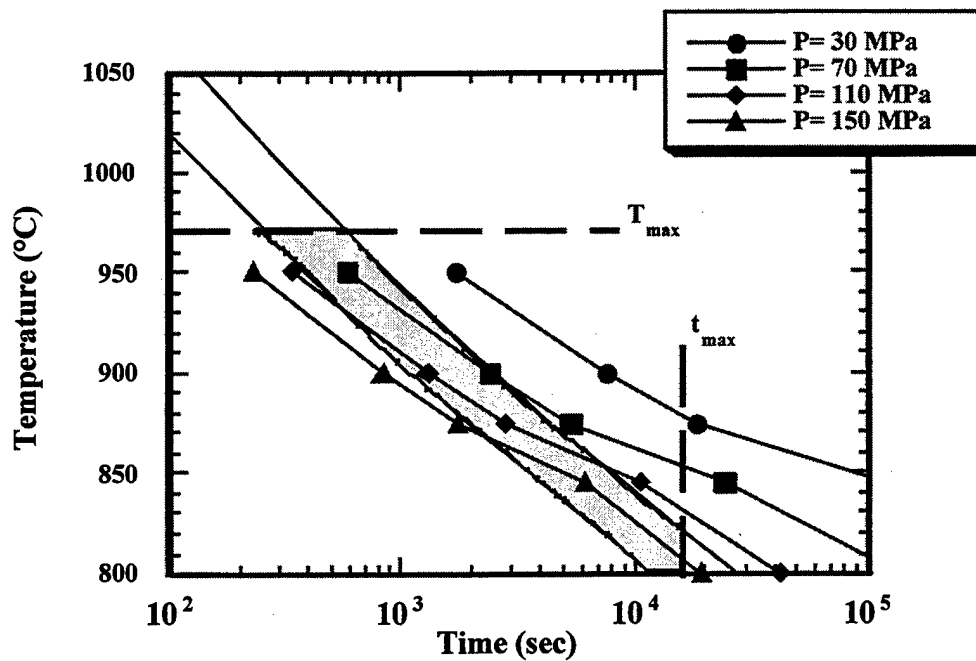


Figure 2-19: Processing map for the selection of parameters to achieve full consolidation of Ti-6Al-4V/SCS-6 MMCs with optimal reaction zone thickness.

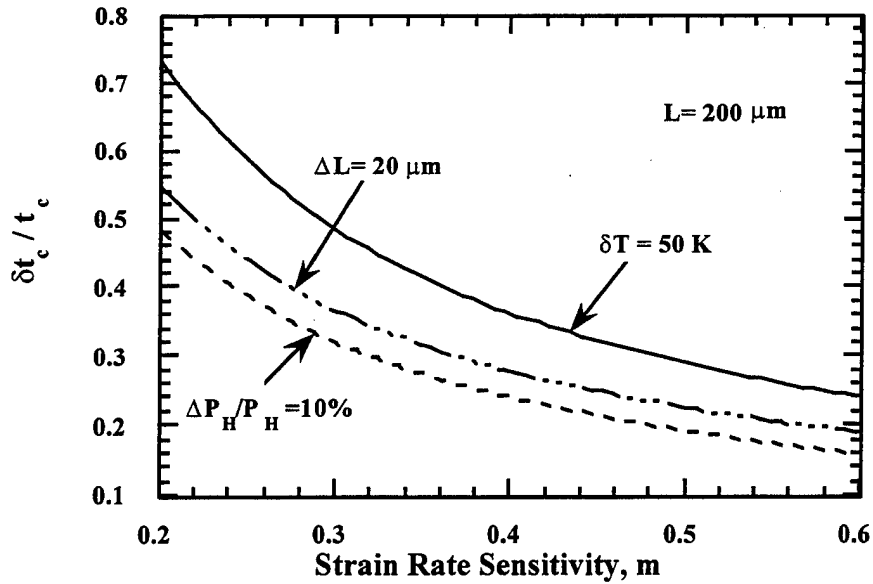


Figure 2-20: Dependence of the consolidation time on the strain rate sensitivity m and fixed variation in processing pressure, temperature, and fiber spacing.

Details of the design of consolidation cycles can be found in the following references:

1. "Design of Metal Matrix Composite Consolidation Practices Based on the Foil/Fiber/Foil Approach", P.D. Nicolaou, S.L. Semiatin, and H.R. Piehler, Scripta Metall. Mater., Vol. 32, pp. 57-62 (1995).
2. "Effect of Material and Process Variability on HIP Consolidation of Continuous Fiber, Metal Matrix Composites", W.H. Zimmer, P.D. Nicolaou, and S.L. Semiatin, Scripta Metall. Mater., Vol. 32, pp. 197-200 (1995).
3. "Effect of Temperature Variability and Fiber-Spacing Variations on HIP Consolidation of Continuous-Fiber, Metal-Matrix Composites from Foil/Fiber/Foil Lay-ups", P.D. Nicolaou, S.L. Semiatin, and W.H. Zimmer, Metallurgical and Materials Transactions A, 26A, pp. 1906-1908 (1995).

2.5 Novel Processing Methods

2.5.1 Equal Channel Angular Extrusion (ECAE)

The broad feasibility of using ECAE for breakdown of (canned) gamma titanium aluminide ingot materials was demonstrated. The workability of these materials during ECAE was shown to be limited by shear localization. For example, a relatively sound product was produced by extrusion at 1250°C of cast plus HIP'ed Ti-45.5Al-2Cr-2Nb canned in type 304 stainless steel, but shear bands and gross shear cracks were developed when extrusion was attempted at 1150°C. These observations were explained in terms of the effect of extrusion temperature on the magnitude of the flow localization parameter in simple shear, or the ratio of the normalized flow softening rate to the strain rate sensitivity exponent. In the cast + HIP'ed condition, the Ti-45.5Al-2Cr-2Nb alloy exhibits a sharp increase in the flow localization parameter and thus susceptibility to shear failure with decreasing temperature. On the other hand, values of the flow localization parameter for Ti-45.5Al-2Cr-2Nb in the wrought condition are somewhat lower, thus suggesting the design of multi-pass ECAE sequences involving an initial high temperature pass for ingot breakdown followed by lower temperature passes for microstructure refinement.

2.5.2 Graded Microstructures by Induction Heating

An induction heating process was designed and developed to obtain graded microstructures in a $\alpha + \beta$ titanium alloy. In this work, Ti-6Al-4V bars, approximately 75 mm in diameter, with an initial microstructure of $\sim 10 \mu\text{m}$ equiaxed grains were heated using an induction coil operating at 4 kHz and 25 kW. For a heating time of 1 minute, the peak surface temperature was estimated to be $\sim 1150^\circ\text{C}$. After cooling, the metallographic analysis of the bars revealed a surface layer of $\sim 12 \text{ mm}$ which contained a fully transformed beta microstructure, whereas the core region was essentially unaffected by the heat treatment. Thus, an induction heating method to develop graded structures consisting of equiaxed

alpha, duplex, and fully transformed structures from the center to the surface of the Ti-6Al-4V bars was successfully demonstrated.

2.5.3 Smart Forging

Smart forging is a variant of the isothermal forging practice and was developed to achieve grain refinement in single phase gamma alloys. This innovation is based on the following experimental trends: (i) dynamically recrystallized grain size varies inversely with the strain rate, and (ii) hot workability increases as grain size is refined. While the ram speed is kept constant during standard isothermal forging, the smart forging method envisages a two-step process with a substantial change in velocity between the two stages. The process begins with a low ram velocity up to a reduction of ~ 50 percent in height of the billet. At this point, a steady state recrystallized structure is generally attained and the workability of the alloy is improved relative to that of the coarse ingot structure. As a result, the ram speed can be increased by one or two orders of magnitude, without the risk of billet cracking. The increase in ram velocity leads to additional grain refinement during the second cycle of recrystallization. The above technique was applied successfully to isoforging of a Ti-51Al-2Mn alloy and a sound forging with a grain size of ~ 30 μm was obtained. Extension of this method to the forging of two-phase titanium aluminides such as Ti-45.5Al-2Nb-2Cr met with limited success, because of the fact that the kinetics of dynamic globularization in coarse grain, fully lamellar structures are very sluggish.

2.5.4 Controlled Dwell Extrusion

Controlled dwell extrusion represents a method designed to overcome the problems associated with the extrusion of a harder billet such as gamma titanium aluminide inside a softer can such as stainless steel or Ti-6Al-4V. At typical extrusion temperatures (1100-1300°C), the flow stress mismatch between the can and the workpiece is so high that nonuniformities in plastic flow occur, leading to can thinning and failure. Sometimes gross fracture of the workpiece results when it contacts the cold tooling.

The 'controlled dwell' approach consists of preheating the canned workpiece in a furnace (or induction heater), removing the assembly from the furnace, and allowing it to air cool for a prespecified, or controlled, dwell period prior to the metalworking operation. The purpose of the controlled dwell is to set up a temperature differential between the can and the workpiece in order to make their respective flow stresses more nearly equal and thus to enhance the uniformity of metal flow during the deformation process. Such a practice contrasts sharply with conventional techniques in which efforts are usually made to minimize the transfer time. The controlled-dwell technique has been applied successfully for the extrusion of several near gamma alloys such as Ti-49.5Al-2.5Nb-1.1Mn and two-phase titanium aluminides such as Ti-45.5Al-2Nb-2Cr. Substantial improvements in the yield of the extruded product were achieved without any gross change in the microstructure of the extrudate. Simple lumped parameter approaches as well as detailed FEM calculations were used to optimize the dwell time.

Additional details regarding this work can be found in the following publications:

1. "Workability of a Gamma Titanium Aluminide Alloy During Equal Channel Angular Extrusion", S.L. Semiatin, V.M. Segal, R.L. Goetz, R.E. Goforth, and T. Hartwig, Scripta Metall. Mater., Vol. 33, p. 535 (1995).
2. "Rapid Heat Treatment of Nonferrous Metals and Alloys to Obtain Graded Microstructures", S.L. Semiatin and D.R. Barker, U.S. Patent 5,429,877 (1995).
3. "A Novel Process for Breakdown Forging of Coarse-Grain Intermetallic Alloys", S.L. Semiatin, P.A. McQuay, and V. Seetharaman, Scripta Metall. Mater., Vol. 29, p. 1235 (1993).
4. "A Simple Analysis for the Design of the Controlled Dwell Extrusion Process", S.L. Semiatin and V. Seetharaman, Scripta Metall. Mater., Vol. 31, p. 1203 (1994).
5. "Controlled Dwell Extrusion Technique for Fabrication of Difficult-to-Process Materials", S.L. Semiatin, V. Seetharaman, R.L. Goetz, and V.K. Jain, U.S. Patent 5,361,477 (1994).

2.6 *Microstructure Evolution Using Cellular Automata*

The computer technique of cellular automata (CA) has been applied to a wide range of problems such as encryption, simulation of forest evolution, lattice gas modeling, and solidification modeling. In the present work, it has been used to analyze the kinetics of static and dynamic recrystallization. CA combines probabilistic and deterministic features to provide a spatial and kinetic description of recrystallization. CA uses a grid of uniform cells that are updated every time step with a finite value or state. CA, as applied to recrystallization, becomes probabilistic through a random choice of cells for nucleation sites. Growth of recrystallized nuclei is governed by cell neighborhoods and a set of deterministic rules. Growth is halted by impingement with surrounding grains.

The main areas of investigation dealt with homogeneous and heterogeneous static recrystallization, and dynamic recrystallization of single phase materials under isothermal conditions. While the majority of this work was carried out using a 2D model, limited work addressed the development of a 3D model. Site saturation and constant rate nucleation were examined for both homogeneous and heterogeneous recrystallization. Homogeneous recrystallization was simulated as a first step to validate the CA algorithm by correlating with Johnson-Mehl-Avrami-Kolmogorov (JMAK) theory, where Avrami exponents of 2 (site saturation) and 3 (constant rate) are expected for 2D growth. The CA algorithm did conform with JMAK theory and the expected Avrami exponents.

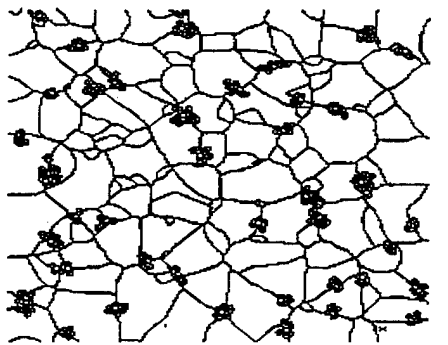
Heterogeneous static recrystallization primarily dealt with grain boundary nucleation. A very limited amount of work concerned the case where two nucleation rates, which differed by an order of magnitude, were applied to two separate regions. This resulted in the formation of a coarse grain microstructure for the lower nucleation rate and a fine grain microstructure for the higher nucleation rate. Grain boundary nucleation was modeled for both site saturation and multiple nucleation events. For site saturation, the fraction of possible grain boundary nucleation sites varied from 0.03 to 0.60. With the

fraction of possible nucleation sites at 0.03, an Avrami exponent of 1.7 was obtained - this is approximately equal to the value of 2.0 obtained for homogeneous nucleation. However, as the fraction is increased to 0.23, the Avrami exponent becomes 1.0, and slightly less than 1.0 for a fraction of 0.60. These results correlate with the work of Cahn for the case when the entire grain boundary area is covered with nuclei.

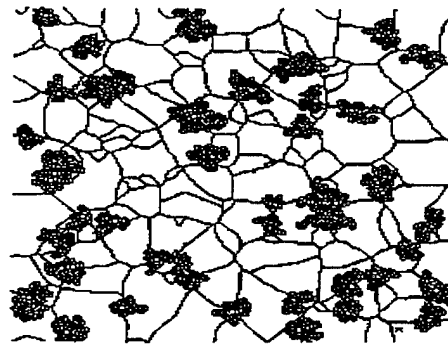
Static grain boundary recrystallization with multiple nucleation events closely resembles the recrystallization of cold worked materials. The CA rules governing grain boundary nucleation placed the first nucleation event at the grain boundaries of the initial microstructure. Further nucleation events were only allowed to occur at the grain boundaries between the newly recrystallized grains and the unrecrystallized regions. Figure 2-21 shows the microstructural evolution for a low nucleation rate, which corresponds to a relatively low level of prior cold work. Microstructures corresponding to three different values (0.05, 0.15, and 0.51) of the volume fraction of recrystallization, F , are illustrated. Figure 2-22 compares the recrystallized structures for three (50, 250, 2000) nucleation rates, N , at a value of $F = 0.50$. The lower nucleation rate results in a clustering of recrystallized grains, while the highest rate leads to a more uniform structure with recrystallized grains decorating the original grain boundaries in the form of a necklace. Avrami plots for this type of recrystallization result in two linear regions and exponents ranging from 1.0 to 1.6.

The CA model of static recrystallization was extended to simulate the dynamic recrystallization process. To account for the strain accumulation in a material as it is deformed, a variable was assigned to each cell to track the dislocation density in the cell. Nucleation was allowed to occur at any randomly chosen grain boundary cell if the dislocation density was greater than or equal to a critical dislocation density. The effect of dislocation storage rate on recrystallization kinetics, grain size, and flow stress curves was examined, as well as the effect of nucleation rate on flow stress curves. Also, the effect of

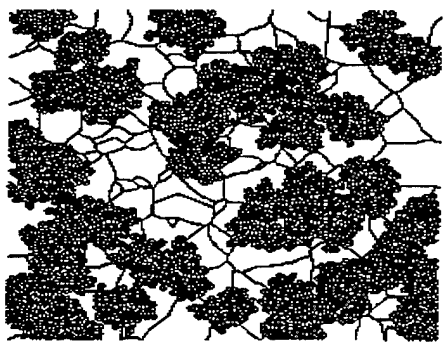
dynamic recovery on the flow curves was examined with and without dynamic recrystallization. Like static recrystallization, the Avrami plot contained bilinear segments with exponents of 1.0 and 2.0. Coarse grain sizes resulted from low dislocation storage rates, and progressively became finer with increases in storage rates. Flow curves displayed a single peak at high rates and oscillations at low rates.



a)

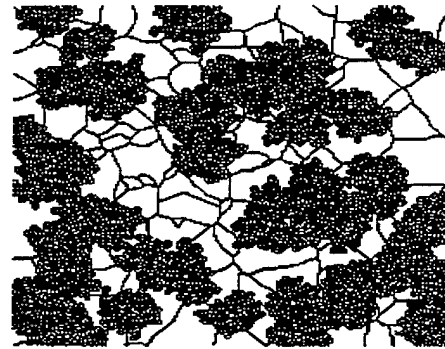


b)

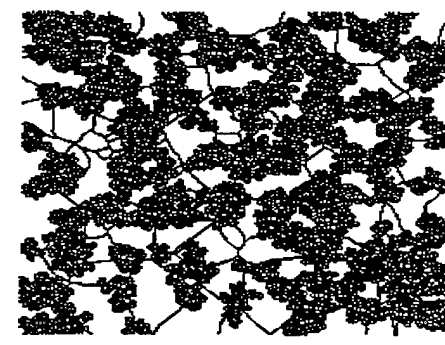


c)

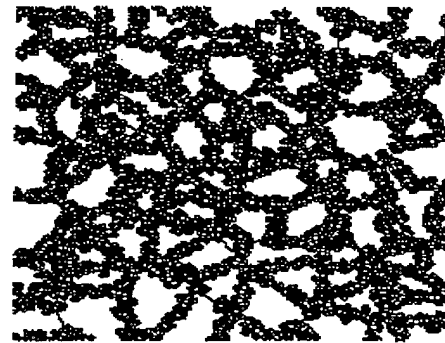
Figure 2-21: Microstructure evolution during static recrystallization.



a)



b)



c)

Figure 2-22: Effect of nucleation rate on static recrystallization.

Further details can be found in the following references:

1. "Static Recrystallization Kinetics with Homogeneous and Heterogeneous Nucleation using a Cellular Automata Model," R.L. Goetz and V. Seetharaman, Metallurgical and Materials Transactions A, in press (1997).
2. "Modeling Dynamic Recrystallization using Cellular Automata," R.L. Goetz and V. Seetharaman, Scripta Materialia, in press (1997).

2.7 Elastic/Plastic FEM Modeling of Tensile and Fracture Test Methods

The finite element method (FEM) was used to model the uniaxial tensile test using an elastic-plastic analysis and a rigid-viscoplastic analysis. The four-point bend test was modeled using an elastic-plastic analysis of a double-notched specimen. The elastic-plastic analyses for the notched tensile test and the four-point bend test were used to rationalize the toughening and fracture processes for Nb and γ -TiAl alloys with the program Nike2d. A Nb-1.24 at. pct. Si alloy notched tensile specimen was modeled at room temperature and -196°C . The principal stresses and effective plastic strains for both conditions show the expected triaxial stress and strain localization (Figure 2-23), which is due to the notch. The room temperature conditions exhibit significant plasticity, however, it only occurs $\sim 700\mu\text{m}$ from the notch tip. At -196°C the strains are much lower and concentrated within $\sim 180\mu\text{m}$ of the notch tip. The results show that fracture is controlled by a combination of strain and axial tensile stress, and that plasticity affects crack nucleation while axial tensile stresses may control crack propagation. Similar results were found in the four-point bend test analysis of Nb and γ -TiAl alloys.

The rigid-viscoplastic analysis of the hot tension test used the program ALPID to compare the FEM necking behavior to a simplified equilibrium approach, and to examine the Bridgman stress triaxiality factor during necking. Several strain rate sensitivities (0.02, 0.05, 0.10,

0.15, 0.20, 0.25, and 0.35) were examined without strain hardening to compare the engineering stress-strain curves of the equilibrium method with the FEM curves. The comparison was very good with the exception of 0.02 and 0.05 strain rate sensitivities, where the equilibrium method predicted a more rapid onset of flow localization. Because the equilibrium method used the Bridgman triaxiality factor, a comparison was made with the FEM estimated values of the triaxiality factor. The greatest divergence between the FEM estimated triaxiality factor and the Bridgman factor occurred in the regions of convex neck profile where the FEM factors were lower. This would cause the equilibrium method to predict flow localization to occur relatively slowly. However, the opposite occurred. This ruled out a difference in the triaxiality factor as the cause for the difference in stress-strain curves. A comparison of axial strain also exhibited similar differences at low rate sensitivities. The difference was eventually explained by the neglect of shear stresses in the equilibrium method.

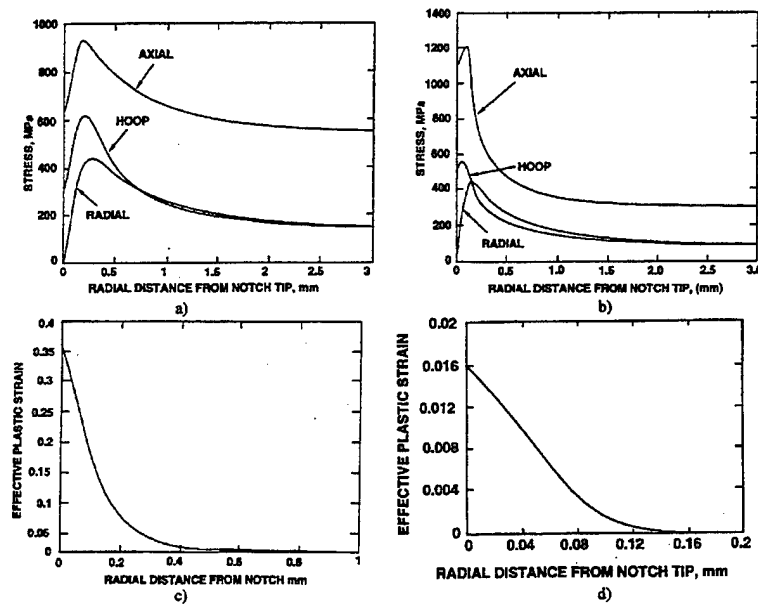


Figure 2-23: Principle tensile stresses and plastic strain vs. distance from notch tip (a) stresses, RT, (b) stresses, -196°C, (c) plastic strain, RT, and (d) plastic strain, -196°C.

Further details on all three areas can be found in the following references:

1. "Unconstrained and Constrained Tensile Flow and Fracture Behavior of an Nb-1.24 At. Pct Si Alloy," M.G. Mendiratta, R.L. Goetz, D.M. Dimiduk, and J.J. Lewandowski, Metallurgical and Materials Transactions A, Vol. 26A, pp. 1767-1776 (1996).
2. "Numerical Analysis of the Hot Tension Test," C.M. Lombard, R.L. Goetz, and S.L. Semiatin, Metallurgical Transactions A, Vol. 24A, pp. 2039-2047 (1993).

2.8 Evaluation of HTC in Deformation & Solidification

An accurate interface heat transfer coefficient (HTC) is an important input parameter of any deformation or solidification FEM model. The HTC greatly affects the heat flow between a billet and die during plastic deformation processes, and also between a casting and mold during solidification processes. For example, many deformation processes are non-isothermal mainly due to the temperature difference between the high temperature billet and low temperature die. This causes temperature gradients in the billet which then causes non-uniform deformation. The HTC in deformation is affected by the lubricant, temperature, interface pressure, and surface roughness. The interface HTC is also a major factor in canned forging, extrusion, and rolling, where the addition of the can/billet interface and any insulators must also be considered. During solidification processes, the HTC is affected by coatings on mold surfaces, temperature, and the phenomenon of "shrink on, shrink off". This phenomenon is caused by the thermal contraction of the cast material, and the casting shape which causes the casting to contract around certain interfaces with the mold (higher HTCs) and shrink away at other interfaces (lower HTCs). Thus, for accurate FEM models, an accurate interface HTC is required for the specific conditions of the deformation and solidification process.

The HTC for deformation processes has been determined using two methods in which temperatures are measured near the interface in the billet and in the die. The relation, $q = h \cdot A(T_{\text{billet}} - T_{\text{die}})$, is used to determine h , the HTC, where A is the contact area, T_{billet} and T_{die} are billet and die interface temperatures, and q is the rate of heat flow. The first method involved a two-die technique to determine the HTC as a function of pressure between workpiece materials of 304 stainless steel and IN718, and die materials of Waspalloy and H13 tool steel. Various interface temperatures and pressures were used for interfaces coated with glass lubricants, a silica fabric, and uncoated. Pressures from 0 to 140 MPa, and temperatures of 980°C and 1090°C resulted in heat transfer coefficients from 0.1 to 15 kW/m² °C. The second method involved the ring test, which allows much larger deformations than are possible with the two-die method. This technique, however, relies on temperature measurements in the die only, and requires some form of numerical model to relate the ring temperature with the die temperature response. The FEM code, DEFORM, was used to determine the interface HTC vs. pressure for various nickel-base superalloy rings lubricated with glass. The results for this work are shown in Figure 2-24.

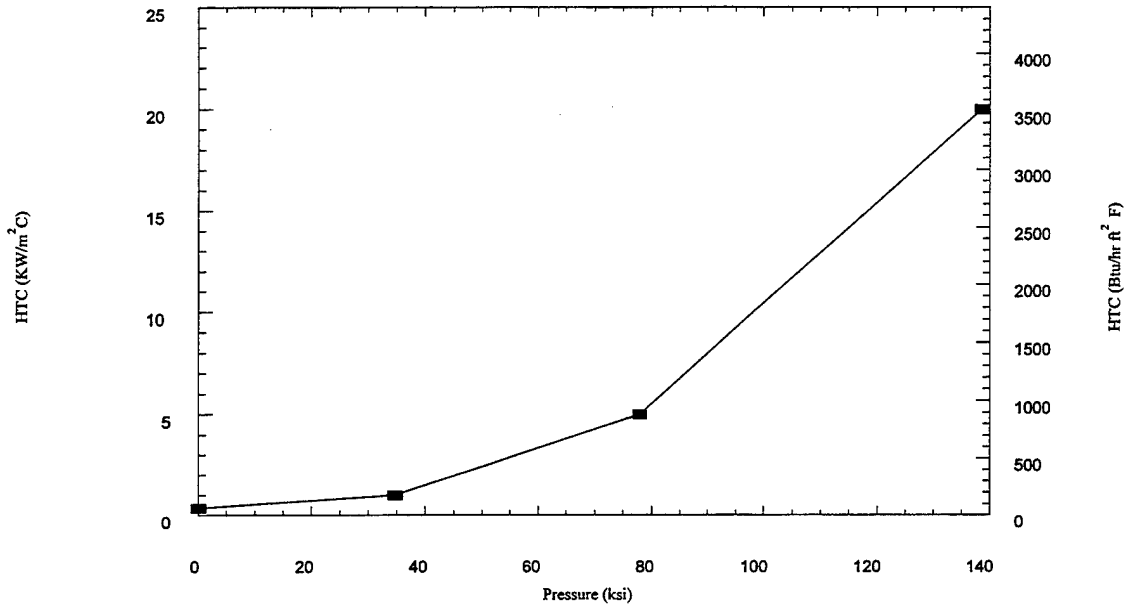


Figure 2-24: Heat transfer coefficient for nickel-base superalloys using the ring test.

Further details on the determination of deformation and solidification HTC's can be found in the reference below.

1. "Determination of Contact Heat Transfer Coefficient for Forging High Temperature Materials," V.K. Jain and R.L. Goetz, presented at the National Heat Transfer Conference, Minneapolis, MN, 28-31 July 1991, ASME 91-HT-34.

3. Modeling Tasks

3.1 *MMC Consolidation Modeling and Experimental Validation*

The consolidation of metal-matrix composites (MMC) using hot isostatic pressing (HIP) of foil-fiber-foil lay-ups was modeled using the finite element program, ALPID. A unit cell approach was used to determine the deformation pattern of various fiber arrangements and consolidation times. For a given fiber architecture, the consolidation time was found to be heavily dependent on the ratio of the HIP pressure to average flow stress and the friction conditions at the matrix-fiber interface. The specific influence of material properties such as the rate sensitivity of the flow stress appears to enter only as a second order effect. The finite element modeling (FEM) solutions were used to construct HIP diagrams for full composite consolidation given combinations of temperature, time, and pressure. Laboratory trials on subscale foil-fiber coupons were used to validate the FEM predictions [3,5].

3.2 *Tensile Test Simulation*

Plastic flow during the round bar, uniaxial tension test was analyzed for conditions representative of the hot-working of metals. The finite element program, ALPID, was used to compare with a simpler finite-difference technique. Variables which were investigated included material properties (strain-hardening exponents of 0 or 0.1; strain-rate sensitivity exponents between 0.02 and 0.30) and tensile bar geometry (tapered, hourglass, and bulged). Results were summarized in terms of engineering stress-strain curves, axial strain distributions after flow localization, and total elongations. The results from the two numerical techniques were similar, due to the *predicted* (FEM) and *assumed* (finite-difference) stress triaxiality during neck formation. The FEM estimated values for the Bridgman triaxiality factor compared well for concave

regions of the neck. However, for convex regions of the neck, the FEM estimated triaxiality factors were noticeable lower than Bridgman factors [4].

3.3 Stress Analysis of TiAl Ingots During Reheating

The development of temperature gradients and thermal stresses during the heating of large ingots was modeled for brittle intermetallic materials such as titanium aluminides. Finite element simulations using ALPID (heat transfer) and Nike2D (stress analysis) were compared to analytical results, which used a series solution for radial temperature transients in conjunction with an elasticity analysis. The FEM techniques featured the ability to model end effects and variations of thermal and elastic properties with temperature, something not possible with the analytical method. The two methods were used to determine the maximum stresses generated during ingot heating. Both methods demonstrated likely brittle fracture when the ingot was charged directly into a 1093°C furnace. However, fracture was not likely when the ingot was first charged into a 649°C furnace for 10 hours and then raised to 1093°C at the rate of 140°C per hour [11].

3.4 Notched Tensile Test Simulation

The finite element method was used to model the uniaxial tensile test using an elastic-plastic analysis (Nike2D) for a notched specimen. The elastic-plastic analysis for the notched tensile test was used to rationalize the toughening and fracture processes for a Nb alloy (Nb-1.24 at. pct. Si). The tensile test was modeled with material properties for room temperature and -196°C. The principle stresses and effective plastic strains for both conditions show the expected triaxial stress and strain localization, which is due to the notch. The room temperature conditions exhibit significant plasticity, however it only occurs ~ 700µm from the notch tip. At

-196°C the strains are much lower and concentrated within ~ 180µm of the notch tip. The results show that fracture is controlled by a combination of strain and axial tensile stress, and that plasticity affects crack nucleation while axial tensile stresses may control crack propagation [9].

3.5 Notched Four Point Bend Test Specimen Simulation

The notch fracture behavior of two γ titanium aluminide alloys, having duplex and fully lamellar microstructures, has been investigated as a function of notch geometry and test temperature using the double notch, four point bend test. The unnotched tensile properties and notch fracture loads were used to perform FEM (Nike2D) analysis to determine triaxial tensile stresses and effective plastic strains in the vicinity of notch roots. These results, together with fractographic examinations of notch failures, indicate that a crack nucleates in the triaxial tensile field when the effective von Mises stress just exceeds the uniaxial tensile yield stress. The high tensile stress component then propagates the nucleated microcrack to failure with local stress intensity reaching the toughness of the material. Thus, both plasticity and high tensile stress are required to cause notch failure [15].

3.6 Uniaxial Upsetting of a Porous Alumina Cylinder using Alpid-PM

This work was a preliminary step to predicting the optimum pressure-time cycle for tape cast composites, where densification is through pressure-sintering. The finite element program ALPID-PM was used for this work. ALPID-PM was modified because it was developed for powder metals and densification by sintering was not included. This work was correlated with the work of K. Venkatachari and R. Raj¹ which dealt with the effect of axial pressure, or time,

¹ Koththavasal R. Venkatachari and Rishi Raj, "Shear Deformation and Densification of Powder Compacts," J. Am. Ceram. Soc., 69, 499-506, 1986 [6].

on axial strain, radial strain, and densification of Alumina cylinders. The cylinder diameters were 15 mm, the height was 20 mm, and the initial relative density was 42 percent.

Densification by sintering was included in ALPID-PM by modifying its constitutive relation: $A \cdot J_2' + B \cdot J_1^2 = Y_R^2 = \delta \cdot Y_0^2$, where J_2' is the second invariant of the deviatoric stress (plastic flow), J_1 is the first invariant or hydrostatic component (densification), and Y_0 is the yield stress of the fully dense material. The parameters A, B, and δ are defined as: $A = 2+R^2$, $B=(1-R^2)/3$, or $B=1-A/3$, and $\delta = R^2-1$, where R is the relative density, ρ_i/ρ_{Dense} . For comparison with three levels of constant axial stress (σ_z) from Venkatachari and Raj, A, B, and δ were modified: (1) $\sigma_z = -19\text{MPa}$, $A=2.4$, $B=0.20$, (2) $\sigma_z = -0.50\text{MPa}$, $A=0.88$, $B=0.71$, (3) $\sigma_z = -1.6\text{MPa}$, $A=2.1228-0.561 \cdot R$, with $\delta = 1/R$ for all cases.

The results compared well with Venkatachari and Raj. The model yielded the following values of axial (ϵ_z) and radial (ϵ_r) strain, $\epsilon_z[\epsilon_r]$: (1) -0.27 [0.05], (2) -0.22 [-0.13], (3) -0.39 [-0.07]. As expected, the axial strains are negative due to compressive loading. In cases 2 and 3 with low pressures and long times, the radial strains are negative indicating contraction. This is caused by densification through sintering comes into play at longer times. In case 1, the axial stress is high, which results in densification in a short time before sintering can occur, and the radial strain is positive. Simulations were also conducted under similar conditions for the pressure-sintering of a cylinder containing a rigid, spherical inclusion.

3.7 Heat Transfer Modeling of MMC Lay-ups Using Alam 1-D Model

This work deals with the hot isostatic pressing (HIP) of the α_2 TiAl alloy, Ti-24Al-11Nb, and SCS-6 SiC fiber metal matrix composite (MMC) using the foil-fiber-foil method. Numerical modeling was initiated to better understand the heat transfer aspects of the process during heating under the 'worst case' conditions of a shielded tool and low seating pressures.

Typically, the MMC lay-up is placed in the cavity of a large steel tool, covered with metal stiffeners and separators, sealed in the tools by welding a steel bladder over the tool cavity, and evacuated. The tool is then placed in a HIP vessel, which is a cylindrical cavity with heating elements on the sides and ends. Multiple tools are suspended in the vessel which causes some tools to be shielded from the heating elements. Temperatures can be taken at the tool surface, however the lay-up temperatures are unknown because the thermal resistance in the lay-up is very high due to the numerous interfaces and small contact areas, no convection due to the evacuated cavity, and low radiation below 700°C. Because of these factors, a 1-D lumped parameter model was developed to predict temperature transients in the lay-ups so that the HIP process can be controlled better [6].

3.8 *Controlled Dwell Canned Forging*

The design of cans to produce uniform, defect-free gamma titanium aluminide alloy pancakes via conventional, nonisothermal forging was established using finite element modeling (DEFORM) and laboratory validation trials. The specific problem addressed was ingot breakdown via pancake forging, a process typically comprising a high reduction ratio (~ 6:1) and a moderately high deformation rate ($\sim 1 \text{ s}^{-1}$) to minimize the effects of die chilling. Can and process variables investigated in the FEM simulations included can end cap shape and thickness, ram speed, and preheat temperature. The FEM results demonstrated that there is an optimal end cap thickness and ram speed to obtain moderately uniform flow between the can and the TiAl workpiece. These results were validated through trials on the near-gamma TiAl alloy Ti-45.5Al-2Cr-2Nb forged in AISI type 304 stainless steel cans [10].

3.9 Al-Li Rolling

Finite element modeling (DEFORM) of multiple pass rolling of Al-Li slabs was performed. This was done under plane strain, nonisothermal conditions. The initial temperature of the slab was 482°C with a reduction of 1.8 mm/pass for 10 passes. The roll temperature was 23°C to simulate rolling on the MPL rolling mill. FEM results included the strain accumulated during each pass, temperature distributions, and roll load.

3.10 Cooling Curve Prediction of Al-Li Cube Using ANTARES™ 3D and Lumped Parameter Model

This work modeled the cooling of an Al-Li cube (27.94 x 27.94 x 31.75 mm) taken from a furnace at 932°C and cooled while suspended in ambient air. An ANTARES™ 3D simulation was conducted as well lumped parameter numerical solutions. The lumped parameter models varied in complexity from a single node to 64 nodes. The lumped parameter model results in a coupled differential equation for each node that is solved numerically using a fourth-order Runge-Kutta technique. The results of all three models compared very well with experimental thermocouple measurements. The lumped parameter time-temperature results were: 200s (775°C), 400s (645°C), 600s (550°C), 800s (470°C), 1000s (410°C), and 1200s (360°C).

3.11 The Effect of Can Shielding During PM HIP Consolidation

This work was performed to investigate the effect of can design on the state of stress during powder consolidation using hot isostatic pressing (HIP). The finite element program DEFORM was used to model the consolidation of an α_2 titanium alloy (Ti-24Al-11Nb) powder in both a 304 stainless steel and mild steel can. Two can geometries were used: (1) an elliptical cross-section under plane strain conditions for HIP cans made of flattened round tubing, and (2)

a cylindrical cross-section under axisymmetric conditions for cylindrical HIP cans with welded end caps. The HIP conditions consisted of 1 and 2 hour consolidations at 1000°C with pressures of 2.07, 6.89, and 68.9 MPa. The can thickness was also varied (3.175, .889, and 1.78 mm). The default PM option of DEFORM was used to determine the relative density distributions in the workpiece, relative density vs. HIP time, workpiece distortion and strain, and state of stress (principal stresses, deviatoric, and hydrostatic). The results were compared to experimental HIP runs for the same conditions. The results showed that can shielding in HIP consolidation of PM materials was of minimal effect.

3.12 GM LCB Ti Forging/Extrusion Simulation for C.V. Joint

This modeling work was performed in support of the cooperative program between General Motors, Wright Laboratory, Wright State University, and UES detailed in Section 4.2.

The finite element modeling used the program DEFORM, and first dealt with the simple, uniaxial upsetting of two sizes of LCB cylinders: (1) 50.8 mm dia. x 76.2 mm long, (2) 40.64 mm dia. x 60.96 mm long. The billets were initially at room temperature. This was in support of preliminary experimental forgings with the MPL 8.9MN press, which indicated a propensity for cracking in half very early in the forging along the shear band. The flow stress used here was supplied by I. Weiss of Wright State University. The ram velocity was 25.4 mm/s. Due to the lack of material data and lack of extensive flow stress data, the modeling did not predict cracking, although it did show adiabatic heating in the center of the billet to 506°C, while the outer surface only reached 117°C.

FEM modeling was also conducted in support of another preliminary step which used the MPL 6.23MN Lombard extrusion press. Since the GM first-stage tooling is a partial extrusion, a die of the same area reduction as the GM tooling was used here, a 120°-included angle, conical

die of 3:1 area reduction. The GM tooling had a 60°-included angle, however. The extrusion press container was 76.2 mm in diameter. Modeling indicated that the load using LCB Ti would be 7.7MN, which exceeds the load limit of the MPL press. Thus, the experimental extrusion was not performed.

The first-stage GM forging uses a billet 49.4 mm in diameter and 126.39 mm long, forged through a 60°-included angle die of 3:1 area reduction. The overall length of the forging is 188.8 mm. Modeling indicated a maximum load of 4.06MN, well within the 8.9MN limit of the Erie press. The maximum effective strain was 1.58. A conical-shaped dimple was formed in the deformed end of the workpiece. This feature was also produced experimentally.

3.13 Extrusion/Forging Simulation of Canned TiAl for GE/AF CRDA Titled, "Texture Development During Gamma Processing"

The finite element method modeling performed here was in support of the GE/AF CRDA on Texture Development During Gamma Processing. The FEM program DEFORM was used for the modeling. The work dealt with the isothermal forging of the near gamma alloy, Ti-45Al-2Cr-2Nb, conventional canned forging of Ti-45Al-2Cr-2Nb and Ti-42Al-2Cr-2Nb, and canned extrusion of Ti-45Al-2Cr-2Nb and Ti-42Al-2Cr-2Nb.

The isothermal forging of Ti-45Al-2Cr-2Nb, which was cast + HIP'ed, was modeled using flow stress from previous Air Force work on cast + HIP'ed Ti-45Al-2Cr-2Nb. The billet diameter was 66.0 mm, the height was 76.2 mm, and the preheat temperature was 1175°C. The ram velocity was 5.1 mm/min. Two friction factors (m) were used, 0.2 and 0.5, to model typical friction conditions and poor lubrication conditions. The billet was forged to a 6:1 reduction. The minimum strain in the dead metal zone was 0.75 ($m = 0.2$) and 0.2 ($m = 0.5$), while the maximum strains were 2.5 ($m = 0.2$) and 3.2 ($m = 0.5$). This indicates that even though both

cases exhibit nonuniform flow, it is greater with higher friction. The strains in the majority of the billet range from 1.4 to 2.0 for the low friction case.

The conventional forging involved the controlled-dwell, canned forging of Ti-45Al-2Cr-2Nb and Ti-42Al-2Cr-2Nb using conventional room temperature dies. The Ti-45Al-2Cr-2Nb alloy was forged with a 304 stainless steel can at a preheat temperature of 1175°C, and with a Ti-6Al-4V can at 1300°C. The Ti-42Al-2Cr-2Nb alloy was also canned in a Ti-6Al-4V can and preheated to 1360°C. In all three cases, the ram velocity was 25 mm/s, and the dwell consisted of a 10s transfer and a 10s free resting period on the bottom die only. The can/billet interface friction factor was 0.6, and the can/die friction factor was 0.2. During forging, the can/billet interface heat transfer coefficient (HTC) was 5.0 kW/m²°C, and the can/die HTC was 20.0 kW/m²°C. At all other times, both HTC's were 0.50 kW/m²°C. Also, the emissivity was 0.65 for both can materials. As with the isothermal forging, the flow stress was from previous Air Force work on cast + HIP'ed Ti-45Al-2Cr-2Nb. The Ti-42Al-2Cr-2Nb flow stress data was obtained through a normalization procedure in which the Ti-45Al-2Cr-2Nb data used, and the temperature of a given stress was lowered 100°C. This procedure was based on previous studies.

All three conventional forgings were given a 6:1 reduction. Also, the billet diameter was 60.5 mm and the height was 86.4 mm. The can thickness was 10 mm with 6.4 mm end caps. The Ti-42Al-2Cr-2Nb alloy, forged at 1360°C with the Ti-6Al-4V can, experienced highly non-uniform deformation. The billet experienced extreme thinning in the region of its central axis, something also shown experimentally. This was caused by an excessive mismatch in flow stress between the can end caps and billet, due to excessive chilling of the end caps and low billet flow stress. At a 6:1 reduction, the minimum and maximum can temperatures were 305°C and 1190°C, while the minimum and maximum billet temperatures were 1042°C and 1358°C. The

billet effective strains ranged from 2.0 to 3.0. The Ti-45Al-2Cr-2Nb alloy, forged at 1175 °C with the 304 stainless steel can, exhibited more uniform can and billet deformation, also shown experimentally. However, the Ti-45Al-2Cr-2Nb alloy forged at 1300°C with the Ti-6Al-4V can did not compare well with the cross-section of the experiment forging, even though the simulation showed similarities with the previous two forgings.

Controlled-dwell canned extrusion simulations were also conducted for Ti-45Al-2Cr-2Nb and Ti-42Al-2Cr-2Nb. Ti-45Al-2Cr-2Nb was extruded at 1300°C with a Ti-6Al-4V can. Ti-42Al-2Cr-2Nb was extruded at 1210°C with a 304 stainless steel can, and at 1360°C with a Ti-6Al-4V can. The same dwell times and interface HTC's were used that were used for the conventional forgings discussed earlier. The can/billet friction factor was 1.0, and the can/die friction factor was 0.35, which is known from previous work to correlate well with glass lubrication. The ram velocity was 25.4 mm/s and the reduction ratio was 6:1. The extrusion press, container and die temperatures were 260°C. The billet diameter was 55.9 mm and the total height was 127 mm. The billet also had a 30°/31.14 mm nose chamfer. The can diameter was 73.66 mm, a height of 101.6 mm, and a thickness of 6.35 mm. The can end cap was 19.05 mm thick, and the nose was a uniform 6.35 mm around the 30° billet chamfer.

The simulation results indicate that the Ti-6Al-4V can in the Ti-42Al-2Cr-2Nb/1360°C extrusion failed. This was also shown experimentally. The can exhibited thinning and a necking down at the die exit very early in the extrusion. The Ti-42Al-2Cr-2Nb/1210°C extrusion with a 304 stainless steel can was successful. Point tracking showed that the center and mid-radius experienced maximum effective strains of 1.4, temperatures of 1257°C, and strain rates of $4.0s^{-1}$. The outer radius, near the can interface, experienced a maximum strain of 2.4 and a strain rate of $8.0s^{-1}$. The outer radius was initially at 1190°C due to chilling, and reaches a peak temperature

of 1275°C due to deformation in the die, before again chilling to 1257°C upon exit from the die. The Ti-45Al-2Cr-2Nb/1300°C/Ti-6Al-4V extrusion shows trends similar to the Ti-42Al-2Cr-2Nb/1210°C. Center and mid-radius strains were 1.2, temperatures peaked at 1343°C from 1290°C, and strain rates were 5.0s⁻¹. The outer radius strain was 1.9 and the strain rate was 7.8. The temperature started at 1244°C and peaked at 1343°C, although not exceeding the center and mid-radius temperatures as with the Ti-42Al-2Cr-2Nb/1210°C extrusion. Can failure was not present in either case, something also shown experimentally.

3.14 Sheet Tensile Test Simulation Evaluating Specimen Shape and Deformation

This work was conducted to evaluate the best specimen shape for sheet tensile tests of superplastic materials. The initial specimen shape included a grip region of comparable width to the gage region, which resulted in excessive elongation in the grip region. The goal was to reduce deformation in the grip region to a minimum by first modeling different shapes using FEM modeling before actual specimens were produced. DEFORM 2D and ANTARES™ 3D were used for the FEM work.

3.15 Equal Channel Angular Extrusion (ECAE) Modeling

The equal channel angular extrusion (ECAE) process was developed in the former Soviet Union, and is being used as an alternative method for the primary breakdown of conventional and advanced alloys. In the process, a workpiece with a square cross-section is pushed down a square channel of equal size and through an angle, which can vary up to 90°, into another channel of the same cross-sectional area. The cross-sectional area of the workpiece is not reduced as in conventional extrusion. With a 90° angle, the partially deformed workpiece would be L-shaped. The amount of deformation (strain) in the workpiece is a function of the angle and the

type of strain is primarily shear. The process enables the use of much smaller starting ingots for ingot breakdown, because the cast structure can be broken up without changing the cross-sectional area. This is an advantage for expensive alloys such as TiAl's.

This work involved the finite element modeling of the ECAE process through a 90° die for a TiAl alloy, Ti-45.5Al-2Cr-2Nb, canned in 304 stainless steel. The billet preheat temperature was 1150°C and 1250°C, while the die temperature was room temperature (23°C). The ram velocity was 25 mm/s, the can/billet interface friction factor was 0.3, and the can/die friction factor was 0.2. During forging, the can/billet interface heat transfer coefficient (HTC) was 5.0 kW/m²°C, and the can/die HTC was 20.0 kW/m²°C. At all other times, both HTC's were 0.50 kW/m²°C. The transfer and die dwell times were 5.0s. The billet was 18.29 mm square and 132.6 mm long. The can thickness was a uniform 3.56 mm. The flow stress was from previous Air Force work on cast + HIP'ed Ti-45Al-2Cr-2Nb.

The results indicated that the can would fail for the 1150°C case. This was caused by the flow stress mismatch, due primarily to the high flow stress of the TiAl billet at this temperature. The can failure occurred at the bottom of the workpiece, in what could be referred to as the 'heel', at a ram stroke of 30 mm. The propensity for can failure in this region was also seen experimentally, where similar deformation occurred. At this point, the maximum strain in the billet was 1.3, with shear bands forming at 45°. The 1250°C extrusion did not suffer can failure, although the can did initially thin slightly in the 'heel' region. The deformation compared very well with experimental extrusions. At a ram stroke of 89.7 mm, the maximum strain was 2.0, although the strain in the majority of the workpiece was 1.0 with the highest strains along the bottom. The maximum strain rate was 3.0s⁻¹ in the shear band. The temperature throughout most of the workpiece was 1287°C, with a maximum of 1301°C and a minimum of 1191°C in

the nose. Due to the 1150°C can failure, it was not possible to obtain results at a large ram stroke. To avoid this, both extrusions (1150°C and 1250°C) were modeled without cans and with very low billet/die interface heat transfer. This was a reasonable solution since the canned billet was insulated and heat loss was minimal. Under these conditions, the 1150°C extrusion displayed severe shear banding that oscillated resulting in a wavy extrusion. The 1250°C extrusion displayed slight shear banding, although not to the degree of the 1150°C extrusion. These results were also shown experimentally with the 1150°C extrusion suffering severe, reoccurring shear band fractures. The 1250°C extrusion only suffered surface fractures at the upper can interface. The shear banding was caused by the low strain rate sensitivity at 1150°C, whereas the rate sensitivity was higher at 1250°C, resulting in more uniform flow.

3.16 Temperature Prediction During MMC Forging Based on Earlier Work

The feasibility of the rapid consolidation of Ti-14Al-21Nb/SCS-6 foil-fiber-foil composites using a forging approach was established as an alternative to slower and more expensive processes such as hot isostatic pressing (HIP), or vacuum hot pressing (VHP). A firm basis for the technique was developed through theoretical analyses of temperature transients, forging pressures, and fiber fracture. Temperature transients have a very strong influence on the flow stress of the matrix foils and thus the pressures required to consolidate the lay-up, the loads applied to the fibers, and the tendency for fiber fracture. A lumped-parameter heat transfer model was developed to quantify temperature-transient behavior. The model consisted of a network of elements separated by thermal resistances of which there were three types: (1) conduction throughout a continuous body, (2) contact interfaces between bodies, and (3) surfaces which lose heat via radiation and convection. The analysis modeled the temperature transients during the seven stages of the process: (a) transfer from furnace, (b) contact with bottom die only, (c) forging and

(d) dwell with contact on both dies, (e) contact with bottom die only, (f) transfer back to furnace, and (g) inside furnace again. The model included 36 segments to account for the dies, the stainless steel can, tantalum foil, and MMC lay-up. This resulted in 36 coupled differential equations which were solved numerically using the fourth-order Runge-Kutta technique. Measurements were made by spot welding a thermocouple on each side of the outer surface of the can. Temperature-transient predictions from the model showed excellent agreement with the measurements [8,12].

3.17 Controlled Dwell G2 TiAl Extrusion Simulations

This work deals with the controlled dwell extrusion of the cast + HIP'ed gamma TiAl alloy, Ti-49.5Al-1.1Mn-2.5Nb, designated G2. The simulations were conducted with two die angles (60° and 120°), three dwell times (0, 30s, and 90s), two preheat temperatures, (1150°C and 1250°C), and various can designs and insulation conditions. The different conditions were chosen to show the advantages of controlled dwell extrusion, predict extrusion failure, and support experimental extrusions performed at Cameron Forged Products, Houston, Texas.

The G2 billets and 304 stainless steel cans were designed with nose chamfers of either 60° or 120°-included angle. The nose angles were chosen to match the angle of the conical extrusion die used. The G2 billet diameter was 55.9 mm and the total height was 127 mm. The can diameter was 73.66 mm, the height was 101.6 mm, and the thickness was 6.35 mm. The can end cap was 19.05 mm thick, and the nose was a uniform 6.35 mm around the 60° or 120° billet chamfer. Table 3-1 lists the simulation conditions and results with respect to can failure.

Table 3-1: G2 TiAl, Controlled Dwell Simulation Parameters

Simulation No.	Temperature (°C)	Die Angle (degree)	Dwell Time (sec.)	HTC during extrusion* (kW/m ² °C)	HTC during dwell (kW/m ² °C)	Results
1	1150	60	30	5/10	0.5	Good
2	1250	60	0	5/10	0.5	Good
3	1250	60	30	5/10	0.5	Good
4	1250	60	90	5/10	0.5	Good
5	1250	120	0	5/10	0.5	Fail
6	1250	120	30	5/10	0.5	Fail
7	1250	120	90	5/10	0.5	Fail
8	1250	60	0	5/10	5.0	Good
9	1250	60	30	0.5/10	0.5	Fail**
10	1250	60	0	0.5/10	No Dwell	Fail***

* Can-core/can-die

** Old Can Design

*** No Container Dwell, Ram Velocity = 25 mm/s, Can/Core Friction Factor, $m = 1.0$, Can/Die Friction Factor, $m = .35$, Container Dwell = 15s.

The simulations show that the 120° die/nose angles result in can failures for all dwell times. The cans were pinched off by the G2 billet. This was caused by the sharp, almost shear die angle. However, this was not shown by extrusions at Cameron. Simulation no.8 approximated the effect of the can/core insulation being removed by using a large HTC (5.0 kW/m²°C) during the dwell period. Simulation no.9 modeled the ‘old’ can design with the square nose on the core. This resulted in can failure, which was shown by Cameron extrusions. Simulations nos. 10 and 2 are comparable in that the dwell time is zero. However, simulation no. 10 resulted in can failure. The difference is that the 15s container dwell was not used in simulation no. 10 and the can/core HTC during extrusion was 0.5 rather than 5.0 kW/m²°C. This would indicate that heat loss to the container is of greater benefit than a dwell period in air for increasing the can flow stress, and equalizing the relative can/core flow stresses. Also note that the low can/core HTC (0.5 kW/m²°C) of simulation no. 10 would result in less heat transferred to the can from the core, lowering the can temperature, and thereby increasing the can flow stress. There was

not enough time for this to occur, and the can nose was pinched off. The only experimental Cameron extrusion with a can failure using a 60° nose/die angle occurred with a dwell of 85s. Those were conditions similar to simulation no. 4, which did not fail.

Thus, comparisons between the simulations and Cameron extrusions are not conclusive with respect to can failure and dwell. The loads for simulations nos. 2 (3.77MN) and 3 (4.52MN) did compare very well with the Cameron extrusions. Deformation heating in simulation no. 3 resulted in a maximum core temperature of 1325°C, a 125° increase from the preheat temperature. Chilling, however, caused the outer radius to drop to 1125°C before increasing at the die exit. The maximum core strains were 1.5-1.6, and the average strain rate was 5.0s⁻¹ with a maximum at the outer radius of 6.9s⁻¹.

3.18 Controlled Dwell Extrusion and Plotting of a γ -TiAl for the AF/GEAE Program, "Efficient Processing of Gamma Titanium Aluminides"

This finite element method modeling work was done in support of the AF/GEAE program titled, "Efficient Processing of Gamma Titanium Aluminides", for which the subcontractor, Wyman-Gordon, performed the actual extrusion and potting work. The objective of the FEM modeling was to provide insight into the canned extrusion and potting operations used in the wrought processing of the prototype jet turbine parts of the AF/GEAE program using the γ -TiAl alloy, Ti-47Al-2Cr-2Nb(at.%). The FEM program, DEFORM, was used in the modeling.

A parametric study of the controlled dwell, canned extrusion consisted of the following included-die angle and dwell times: (1) 120°/50s, (2) 60°/0s, (3) 60°/45s, and (4) 60°/200s. The initial condition was: a billet temperature of 1316°C, extrusion container temperature of 260°C, ram speed of 17.0 mm/s, billet diameter of 190.5 mm, can diameter of 228.6 mm, can material of Ti-6Al-2Sn-4Zr-2Mo, and reduction ratio of 4:1. The interface heat transfer coefficients

(HTC's) were $5.0 \text{ kW/m}^2\text{K}$ (can/billet), $20.0 \text{ kW/m}^2\text{K}$ (can/die), and $0.50 \text{ kW/m}^2\text{K}$ (transfer and dwell periods). The can/billet interface friction factor was 1.0, and the can/die friction factor was 0.35.

The loads for the $120^\circ/50\text{s}$ and $60^\circ/200\text{s}$ cases were predicted to exceed the maximum 22.24 (MN) load of the Wyman-Gordon R&D press in Houston, Texas. In addition, extreme can thinning occurred in the cases of $120^\circ/50\text{s}$ and $60^\circ/0\text{s}$, although more uniform flow occurred for $60^\circ/45\text{s}$ and $60^\circ/200\text{s}$. Thus, it would seem that a die of 60° and a dwell in air of 45s is optimal. For this case, the TiAl billet experienced deformation heating with maximum temperatures of 1353°C and surface temperatures of $\sim 1250^\circ\text{C}$. The strain in the billet was nonuniform radially, although the final effective strains upon exit from the die were ~ 1.0 throughout.

The forging operation, "potting", is essentially blind upsetting of a billet, canned in this case, in a larger diameter die. There were three FEM simulations performed. The first two used "typical" HTC's for the forging phase (can/billet-5.0, can/die-20.0 $\text{kW/m}^2\text{K}$) with height reductions of 30 and 50 percent. The third used "lower" HTC's ($1.0/5.0 \text{ kW/m}^2\text{K}$) for a 30 percent reduction. This simulated extra insulation at the billet/can interface. During the transfer and dwell periods, all HTC's were $0.5 \text{ kW/m}^2\text{K}$. The can/billet interface friction factor was 1.0, and the can/die friction factor was 0.35. The TiAl billet diameter was 88.9 mm and the height was 254 mm. The 304 stainless steel can was 6.35 mm thick, and the die diameter was 143.5 mm (50 percent reduction) and 121.4 mm (30 percent reduction). The billet preheat temperature was 1204°C and the dies were at room temperature (20°C). The transfer time was 20s and the ram speed was 25.4 mm/s. The predicted loads in all three cases were $\sim 1.957 \text{ MN}$, well within the 22.24 MN load limit. The can deformation was relatively uniform, however, the TiAl experienced a dead metal zone with effective strains of only 0.2, compared with strains of 1.0 in the

billet center (50 percent/typical HTC). The temperature variations for this case were 1075°C to 1230°C. For a reduction of 30 percent, the strains varied from 0.25 to 0.40, and the temperature varied from 1150°C to 1230°C. As expected, the variations are smaller for the case with lower HTC's.

3.19 Valve Forging of Canned/TiAl

The nonisothermal forging of automotive-type poppet valves using γ -TiAl was simulated using the finite element program DEFORM 2D. Experimental forgings resulted in excessive cracking in the stem region of the valve, similar to fir-tree type cracks in extrusions. This is an extrusion-like process in which the valve stem is forged by extruding the cylindrical workpiece through a die of smaller diameter. It was hoped that FEM modeling could show the cause of the cracks by determining the state of stress and temperature of the workpiece. The Ti-46Al-x-x workpiece was surrounded by a Ti-6Al-4V ring that was left on the workpiece after it was extruded during the ingot breakdown stage. The ring protects the γ -TiAl workpiece from die chilling and the effects of friction at the die interface. The γ -TiAl workpiece diameter was 21.2 mm, the height was 27.9 mm, and the Ti-6Al-4V outer ring was 2.1 mm thick. The ends of the workpiece were only covered with glass lubricant. The die exit diameter was 8.61 mm. The initial workpiece temperature was 1204°C, and the die temperature was 200°C. Excessive deformation and thinning of the Ti-6Al-4V ring well before the workpiece exited the die resulted in the γ -TiAl workpiece coming into contact with the die wall. With brittle alloys such as the γ -TiAl's, this is the likely source of the stem cracks. The excessive ring deformation prevented further modeling.

3.20 Heat Transfer Modeling of a Subscale TiAl Disk During Heating and Cooling

The heating and cooling of a subscale γ -TiAl (Ti-45.5Al-2Cr-2Nb) turbine disk was modeled using the heat transfer module of DEFORM. The disk radius was 57.8 mm, the thickness varied from 10 to 14 mm, and the top and bottom ribs were 7.8 and 8.8 mm tall at a radius of ~ 25 mm. Temperature distributions vs. time were determined for radiation emissivities of 0.4, 0.6, and 0.8. For cooling, the disk was at a uniform 1321°C. Two initial temperatures were used for the heating simulations, 1125°C and 1260°C, with the disk placed in a 1321°C environment in both cases. At an initial temperature of 1260°C and an emissivity of 0.6, the disk had maximum temperature of 1320°C and a minimum temperature of 1318°C after 2 minutes.

3.21 Subscale Disk Forging

The forging of a subscale disk was modeled using DEFORM 2D to optimize the preform diameter and height for the γ -TiAl alloy, Ti-47Al-2Cr-2Nb. The required disk geometry is the same as the subscale disk used in the heat transfer modeling discussed above in Section 3.20. The preform diameter and height were optimized to obtain complete die fill with a minimum of flash and avoidance of lap formation. Three preform geometries were examined: (1) 100 mm dia. - 20 mm height, (2) 72 mm dia. - 38 mm height, and (3) 80 mm dia. - 30 mm height. The first preform produced a large amount of flash and filled the rib very late in the forging. The second preform, with a smaller diameter, filled the rib areas early, however the larger height caused a lap to form at the outer diameter before the flash was formed. The third preform, with a smaller height than the second preform and a smaller diameter than the first, filled the ribs without a large amount of flash and without lap formation. There was still a tendency for lap forma-

tion, however, it was nullified by the flash. Thus, the third preform was chosen as the optimal shape.

3.22 Deformation of Single Powder Particle Using ANTARES 3D

This work dealt with the deformation of individual powder metallurgy (PM) particles during a combination of hot isostatic pressing and unconstrained uniaxial upsetting. The goal was to determine the particle height, width, contact areas, and contact pressures during the different states of applied stress present for HIP'ing (hydrostatic) and uniaxial compression (uniaxial). The deformation of a single powder particle was modeled using DEFORM 2D and ANTARES™ 3D. The initial relative density of ideally packed particles was 52 percent and due to symmetry, only one-eighth of the particle was required for modeling. The initial particle radius was 5.0 mm. To simulate HIP'ing, one-eighth of the particle was deformed into the corner of a cube to 63 percent relative density by applying equal normal velocities to its three symmetry surfaces. Then, to simulate unconstrained uniaxial upsetting to 82 percent relative density, a normal velocity was only applied to one of the symmetry surfaces. At this point, the particle had an axial contact radius of 3.2 mm, a transverse contact radius of 2.17 mm, an axial radius of 3.67 mm, and transverse radius of 4.69 mm.

3.23 Publications and Patents on Modeling Tasks

1. "Effect of Core Insulation on the Quality of the Extrudate in Canned Extrusions of γ -Titanium Aluminide," R.L. Goetz, V.K. Jain, and C.M. Lombard, Journal of Materials Processing Technology, 35, pp. 37-60 (1992).

2. "Application of Computer Methods to the Design and Analysis of Precision Rib-Web Forgings," V.K. Jain, R.L. Goetz, and C.M. Lombard, Journal of Materials Processing Technology, 36, pp. 1-16 (1992).
3. "Consolidation of Continuous Fiber Intermetallic Matrix Composites," S.L. Semiatin, R.L. Goetz, and W.R. Kerr, Intermetallic Matrix Composites II, D.B. Miracle, D.L. Anton, and J.A. Graves, eds., Materials Research Society, Vol. 273, pp. 351-364 (1992).
4. "Numerical Analysis of the Hot Tension Test," C.M. Lombard, R.L. Goetz, and S.L. Semiatin, Metallurgical Transactions A, Vol. 24A, pp. 2039-2047 (1993).
5. "Modeling of the Consolidation of Continuous-Fiber Metal-Matrix Composites via Foil-Fiber-Foil Techniques," R.L. Goetz, W.R. Kerr, and S.L. Semiatin, Journal of Materials Engineering and Performance, Vol. 2, No. 3, pp. 333-340 (1993).
6. "Heat Transfer and Plasticity Modeling of Foil-Fiber-Foil MMC Consolidation," R. L. Goetz and M.K. Alam, Proc. Titanium Matrix Composites Workshop, P.R. Smith and W.C. Revelos, eds., WL-TR-93-4105, La Jolla CA (1993).
7. "Workability of a Gamma Titanium Aluminide Alloy During Equal Channel Angular Extrusion," S.L. Semiatin, V.M. Segal, R.L. Goetz, R.E. Goforth, and T. Hartwig, Scripta Metallurgical, Vol. 33, No. 4, pp. 535-540 (1995).
8. "A Forging Technique for the Rapid Consolidation of Continuous Fiber, Metal-Matrix Composites," P.D. Nicolaou, S.L. Semiatin, and R.L. Goetz, Recent Advances in Titanium Metal Matrix Composites, F.H. Froes and J. Storer, eds., TMS (1995).
9. "Unconstrained and Constrained Tensile Flow and Fracture Behavior of an Nb-1.24 Pct. Si Alloy," M.G. Mendiratta, R.L. Goetz, D.M. Dimiduk, and J.J. Lewandowski, Metallurgical and Materials Transactions A, Vol. 26A, pp. 1767-1776 (1995).

10. "Can Design for Nonisothermal Pancake Forging of Gamma Titanium Aluminide Alloys," V.K. Jain, R.L. Goetz, and S.L. Semiatin, Trans. ASME, J. Eng. Industry, Vol. 118, pp. 155-160 (1996).
11. "Modeling of Thermal Stresses and Thermal Cracking During Heating of Large Ingots," M.K. Alam, R.L. Goetz, and S.L. Semiatin, Trans. ASME, J. Manf. Sci. and Eng., Vol. 118, pp. 235-243 (1996).
12. "An Experimental and Theoretical Investigation of the Rapid Consolidation of Continuously Reinforced, Metal-Matrix Composites," P.D. Nicolaou, S.L. Semiatin, and R.L. Goetz, Metallurgical and Materials Transactions A, Vol. 27A, pp. 1719-1730 (1996).
13. "A Simple Analysis of the Hot Consolidation of Metal Matrix Composite Panels from Tape Cast Monotape Lay-ups," S.L. Semiatin, R.E. Dutton, and R.L. Goetz, Scripta Materialia, Vol. 35, No. 7, pp. 855-860 (1996).
14. "Validation of Computer Models for the Consolidation of Metal-Matrix Composites," R.E. Dutton, S.L. Semiatin, and R.L. Goetz, Materials Science and Engineering, 1996 (in press).
15. "Notch Fracture in γ -Titanium Aluminides," M.G. Mendiratta, R.L. Goetz, and D.M. Dimiduk, Metallurgical and Materials Transactions A, 1996 (in press).
16. Controlled Dwell Extrusion of Difficult-To-Work Alloys, S.L. Semiatin, V. Seetharaman, R.L. Goetz, and V.K. Jain, United States Patent, Patent No. 5,361,477, November 8, 1994.

4. Cooperative Projects

4.1 *Gamma Conversion Program*

Permanent mold casting (PMC) is a new casting process for titanium alloys that has the potential to provide lower costs, shorter lead times, and improved process quality when compared to conventional manufacturing methods. The PMC process involves the casting of titanium alloys into reusable metal molds that are resistant to erosion and reaction with molten titanium. Observed benefits, including improved product quality, are a direct result of process simplification through elimination of processing steps.

In the current task, a technical effort was undertaken to start identifying permanent mold cast processing and finishing procedures for producing gamma titanium aluminide components. The technical effort for this task was conducted by UES, Howmet and Pratt & Whitney.

The technical program consisted of two subtasks. Subtask 1 was Process Refinement and concentrated on refining permanent mold processes that affect the solidification of the cast TiAl such as die design, melting method, and pressure injection. Subtask 2 was Casting Demonstration in which a component was selected and produced. The demonstration component was selected jointly by UES, Howmet, Pratt & Whitney and the Air Force. The primary component was an inner stator support. A nozzle tile was selected as a secondary component that would be examined if time and resources permitted.

A great deal of work was completed on this program culminating in the successful casting of the demonstration inner stator support. Evaluation of the cast components and a fully detailed report are expected to be funded and completed as a follow-on effort.

4.2 General Motors Constant Velocity Joint Project

A cooperative program was conducted to investigate and demonstrate the feasibility of fabricating automotive Constant Velocity (CV) joints from a low cost beta titanium alloy (LCB Ti). This was a joint effort involving engineers, scientists and technicians from General Motors Saginaw Division, Wright Laboratory, Wright State University, and UES.

The CV joint is a relatively heavy steel part, so substantial weight savings could be accomplished by successful conversion to a lighter weight titanium alloy. This would in turn result in reduced fuel consumption. The recent development of low cost beta titanium alloys has the potential to substantially reduce the material cost of titanium. A major factor in the cost/performance equation will then be the cost of fabrication. The existing steel CV joint requires a complex production process involving four separate forming operations and extensive heat treatments, so it is an excellent candidate for conversion to titanium alloy.

The approach of the program was to use a scientific methodology to evaluate the inherent workability of LCB Ti, develop a fabrication sequence and demonstrate that sequence on the 1000 ton forge press in the MPL.

GM shipped an 8000 lb. production die stack from one of their Saginaw presses to the MPL. Installing this die stack required a substantial effort to adapt it to our particular press beds and to jury rig a method of using our 200 ton bottom cushion as an ejector. Meanwhile, a series of upset tests were performed to evaluate the workability of the material and numerical modeling was done to predict the loads that would occur in forming (see Section 3.12). We found that proper heat treatment was critical to transforming the LCB Ti from an explosively brittle material to one with room temperature formability.

Working with the government project engineer, we hypothesized that the standard 1500°F heat treatment was not good enough to give a Beta anneal. This conclusion was based on two key points. First, it was noted that the heat treatment temperature on one of the LCB Ti billets was actually above the 1500°F set point and this billet forged well. Secondly, the microstructure of a fractured billet showed a great deal of alpha.

A heat treatment study was conducted to determine proper conditions for achieving a complete Beta structure in the LCB Ti. A higher temperature (1550°F) followed by a water quench was found to give a good Beta structure with minimal precipitation. Thermocouples were imbedded in the center of the billets to determine exactly how long a hold time was needed to get the entire billet to temperature.

Using the new heat treatment method, we successfully performed a room temperature, stage one forging of the CV joint. We then received a long awaited, new batch of LCB Ti from Timet. This new batch was nominally the same composition and had the same processing history. Unfortunately, it behaved quite differently from the original material. We were not able to forge it at room temperature, and instead devised a warm forming scheme. Although this was a frustrating turn of events for our in-house researchers, it still satisfied the original goal of demonstrating the feasibility of forming a CV joint from titanium.

A meeting was held at WPAFB to present results and formulate plans for any future relationship with GM. The results of the Constant Velocity (CV) Joint work performed in the MPL were summarized. The feasibility of forming a CV Joint out of LCB Titanium was demonstrated by the cold and warm forming of the stage one component using two different batches of material. Several potential manufacturing approaches were presented. The GM design engineer at the meeting expressed great interest in these results. We had achieved the goal of demon-

strating the feasibility of replacing conventional steel parts with aerospace materials in order to trim component weight.

4.3 *Ti-Sn Cooperative Project with Naval Surface Warfare Center*

Ti-Sn alloys have been found on a laboratory scale to have high damping over a wide range of frequencies at room temperature.² Those studies were performed on alloys consisting of a Ti₃Sn matrix with an alpha Ti discrete second phase. Samples were arc melted into disc-shaped ingots (buttons) using the highest purity components that were reasonably available. Samples were annealed at 1350°C for 20 hours in argon filled SiO₂ ampoules with a small piece of Y to getter oxygen.

The Navy is interested in determining whether Ti-Sn alloys warrant further investigation. Potential uses include stiffeners in hollow Ti components to reduce solid body vibrations and washers and joint interlayers to dampen hard points caused by fasteners.

The purpose of the current project is to determine if the high damping properties of Ti-Sn alloys made on a laboratory scale can be reproduced on a larger scale. This will also require ascertaining the effect of processing on the damping characteristics and microstructure. The basic mechanical properties of the material must also be determined.

The Air Force role in this project was to determine the processing conditions required to work the as cast material and to then extrude a 3-inch diameter ingot. Compression testing and metallography were performed on the as received material to determine the optimal processing conditions. The as cast ingot suffered from gross inhomogeneity as evidenced by pockets of incipient melting in the high temperature compression tests. After a homogenizing heat treatment,

² C.R. Wong and R.L. Fisher, "Low Frequency Damping and Ultrasonic Attenuation in Ti₃Sn Based Alloys," J. of Materials Research, 9(6), pp. 1441, June 1994.

the material was considerably more workable. An initial extrusion of an uncanned billet suffered from extensive fracture, most probably caused by temperature loss from the billet during loading and extrusion. A second extrusion was performed using the insulated can technique that has been so successful for Ti-Al alloys. This canned extrusion was a success and the material was shipped to the Navy for further evaluation.

4.4 Inco 625 Sheet Rolling for F118-101 Test Program

GE Aircraft Engines requested Wright Laboratory to assist their High Cycle Fatigue testing program. A fatigue failure problem had cropped up in recent engine tests. An Inco-625 oil line feeding the main engine bearing had failed in several engine stand tests at a 90° bend. The tubing is typically cold formed to its service shape. This alloy has been used successfully for many years for oil lines in engines, but there is no fatigue data available for the cold worked state. Now that there was a problem, GE needed to quickly quantify the fatigue behavior of the material in the cold worked condition, so that the oil line design and/or fabrication process could be redesigned.

GE supplied sheet samples 0.038" thick. We used the two high rolling mill in the MPL to cold work the sheet samples to a final thickness of 0.028", which approximates the strain incurred during the cold bending of the oil line tubing. These samples were then returned to GE for machining and fatigue testing.

4.5 Silver-Graphite Extrusion for CMW, Inc.

CMW is an Indianapolis based company specializing in the fabrication of electrical contacts. They do much of their work using their own 700 ton extrusion press. In response to competition from Europe, CMW is attempting to develop an extrusion process for Ag-C (silver-

graphite). Such a material has been used in some contacts in Europe as a replacement for Ag-CdO (silver-cadmium oxide) which is known to release toxic fumes in service. CMW wants to push the graphite content much higher than has been previously extruded, in order to make a higher power contact. They have, as yet, been unsuccessful.

CMW was made aware of the extrusion expertise at the AF Materials Directorate by the National Technology Transfer Center. UES and Government engineers met with CMW's Senior Materials Manager and devised an extrusion processing plan that differed significantly from what CMW had previously attempted. The new technique utilized co-extrusion of the powdered material in a sacrificial can. This technique is commonly used at the MPL for difficult to form materials, so our personnel were already familiar with the required tooling design and processing techniques. CMW provided two billets, both of which were successfully extruded at the MPL.

CMW conducted electrical tests on the resulting material and did find some promising results. At low current, the material surpassed all other materials that they had tested for erosion rate, heating and contact resistance. At higher amperages, the material did not perform well by itself, but did perform well when mated against a contact with high arc quenching capabilities.

This project was a good demonstration of how the expertise and equipment resident in the AF Materials Directorate can be used to assist U.S. industry with a minimal expenditure of manpower and equipment time.

4.6 *Tantalum Alloy Extrusions for Department of Energy Program*

Bechtel Nevada Corporation (Formerly EG&G), under Department of Energy contract, was required to produce large rectangular bar stock of T-222 for subsequent rolling to sheet. This tantalum-hafnium-molybdenum alloy requires a molybdenum can to protect it from oxida-

tion at the 3000°F forming temperature. The full scale production billet dimensions are 10 inch diameter by 36 inch length. The material cost per production billet is approximately \$500,000.

The extrusion subcontractor (Extrusion Technology Company of America) had proposed using a flat faced shear die with a glass pad. They had selected this method because it was what they typically used for Ti extrusions. Fortunately, a consultant on the project, who was familiar with the extrusion expertise at the AF Materials Directorate, suggested doing a subscale trial at the MPL.

The subscale trial using the flat faced shear die and glass pad technique was a failure. The MPL personnel, who have extensive experience with refractory alloy extrusion, recommended an alternate extrusion method using a conical die. The conical die method was a success.

Based on the success of the conical die method in the subscale extrusion, Bechtel decided to go ahead with this method on a production scale. They switched extrusion subcontractors to CSM, Inc. UES personnel worked closely with CSM to assure that the extrusion conditions would match those of the subscale process, even to the point of mixing up a batch of glass lubricant and shipping it to CSM. On April 13, 1996, the first full scale T-222 billet was successfully extruded. Several more such extrusions are scheduled.

4.7 Extrusion of ODS Molybdenum for USDOE & Pittsburgh Materials Technology Inc.

Pittsburgh Materials Technology, working under a USDOE sponsored program (Prime Contract DE-AC11-93PN38195), requested assistance from the Materials Processing Laboratory (MPL) in the forming of an Oxide Dispersion Strengthened (ODS) molybdenum alloy.

The objective of the DOE program is the development of high temperature creep resistant molybdenum alloys in tubular form. The ODS strengthening mechanism selected for investigation is achieved by fine oxide particles stabilizing a deformation structure. The viability of the approach had been indicated by uniaxial creep tests obtained during scoping evaluations of material processed by a combination of hot swaging and drawing. The ODS-Mo creep behavior was superior even to Mo-6Nb single crystal material, a Russian developed material which had been claimed to be the highest strength form of moly above 2500°F.

Investigation into the effects of deformation processing on the mechanical behavior of ODS-Mo alloys required the processing of larger billets, using processing methods likely to be used in full scale production. The extrusion of 3-inch diameter billets was the next logical step in the development program. The instrumented 700 ton extrusion press at the MPL was considered by Pittsburgh Material Technology to be the only source acceptable for this critical DOE sponsored program.

In June 1992, Pittsburgh Materials Technology provided four billets of ODS-Mo, along with extrusion dies and mandrels fabricated as per our instructions. Two billets were for hollow extrusion and two were for solid extrusion. The two solids were extruded successfully at 1400°C - 1500°C. The hollow extrusions were regarded by the MPL personnel as a bit of a long shot and, indeed, neither was successfully extruded. One of the supplied billets expanded asymmetrically on heat up and would not fit over the mandrel, so it was set aside for future work. The other hollow billet went through the extrusion die but seized the mandrel and pulled the mandrel apart. Seizing the mandrel and pulling it apart in tension may have been aggravated by the high extrusion ratio that was being used for this extrusion.

In November 1992, four more billets and dies were provided representing each of two fabrication methods that were under consideration. One pair had been fabricated using a powder metallurgy pressing and sintering approach. The other pair had been press and sintered and then double vacuum arc melted. All four of these billets were successfully extruded.

4.8 Extrusion of High Temperature Alloys for USDOE & Pittsburgh Materials Technology Inc.

Pittsburgh Materials Technology, working under a USDOE sponsored program (Prime Contract DE-AC11-93PN38195), requested assistance from the Materials Processing Laboratory (MPL) in the forming of a number of high temperature alloys that are being evaluated for potential application as a high temperature radiator in a Naval reactor system. The candidate refractory metal alloys are:

- Ta-10W
- T-222 (Ta-10W-2.5Hf-0.01C)
- ASTAR A811C (Ta-8W-1Re-0.85Hf-0.025°C)
- WC-103 (Nb-10Hf-1Ti)
- FS-85 (Nb-27.5Ta-11W-0.85Zr)
- PWC-11 (Nb-1Zr-0.1C)
- Mo-14Re

The selected material must operate in a pressurized environment at relatively high temperature for extended periods of time. Thus, the long term creep behavior is a major concern and will be a primary factor in down-selecting the candidate materials.

Biaxial creep testing will be used to evaluate creep behavior. The specimens will be fabricated from small diameter, thin walled tubing with welded end caps into which an inert gas is

introduced at a specified pressure and the specimen sealed. The specimens are then exposed to various time-temperature combinations in high vacuum, and their changes in diameter and length periodically measured to permit determination of circumferential and axial creep strain as a function of temperature, time and stress (i.e., internal pressure).

A key element in this program was the extrusion of ingots of these candidate materials into round bar stock, which could then be swaged and machined to form hollow tubes and drawn down to thin-walled tubing sizes required for the biaxial creep test specimens. The high cost of these materials made 100 percent success all the more important. The Materials Processing Laboratory (MPL) has had extensive experience in the high temperature extrusion of refractory alloys. The first batch of billets were all extruded successfully. Two more batches of billets are expected during the follow-on to the current MPL contract.

4.9 Co-Extrusion of Dual Alloy Billets for DynaMet

A cooperative program was undertaken with DynaMet Incorporated to investigate the co-extrusion and subsequent drawing of wire of Ti in Cu, Nb-Ti in Cu and Nitinol in Ti. DynaMet was interested in potential applications in orthodontics and orthopedics. The Nitinol in Ti is considered to have the most commercial potential. DynaMet requested the Materials Directorate's assistance because of the considerable experience the Materials Processing Laboratory (MPL) has in co-extrusion of a broad range of materials.

Ten canned billets were prepared by DynaMet to specifications provided by the MPL personnel. All of the billets were successfully extruded in March 1993. The Nitinol in Cu bars were then direct drawn by DynaMet down to 0.031 inch wire in approximately 25 steps. Subsequent analysis showed a porous interface had developed between the Nitinol and the Cu due to the repeated annealing between each of the cold drawing steps. Though this porous layer may

compromise the integrity of the prototype wire, the project was considered a successful proof of concept.

4.10 Rolling Program with Ohio Advanced Technology Center

The Ohio Advanced Technology Center (OATC) contacted the Materials Directorate with a request for assistance in the development of a radical new approach to the processing of flour dough. Though the subject material was outside the normal realm of experience in the Materials Processing Laboratory, the two-high rolling mill was just what the OATC researcher needed for a proof of concept experiment. Like many of the metallic materials we deal with, flour dough requires a certain level of deformation processing (kneading). Even in modern production facilities, this work is imparted in a batch process, just as it has been for thousands of years. By using a rolling mill to impart the work into the flour dough, the leap could be made to continuous processing.

The MPL contribution to this program was very limited (two mornings on the rolling mill), but the results for the OATC researcher were terrific. Based on these trials, a pilot plant facility has been designed and is expected to be rolling dough in the near future.

5. Processing of Materials

Much of the day-to-day activity under this program was focused on the actual processing of materials by either deformation or solidification. This work supported the contractual effort research activities as well as the activities of numerous other agencies both inside and outside of the government. Summaries of these processing operations are given in the following subsections. Complete records were maintained on every major operation performed and are kept on file in the Materials Processing Lab (MPL) office.

5.1 Extrusion

The 700-ton Lombard extrusion press was the most heavily used piece of equipment in the lab. Despite the slow start caused by the lab relocation and man-hours spent on debugging the newly renovated press, 244 extrusions were performed under this program. Customers included several groups in Wright Laboratory as well as many private corporations.

Table 5-1 gives a breakdown of the extrusions performed cross tabulated by Agency versus Material. Detailed records of each operation are on file in the MPL office.

Table 5-1: Summary of Extrusions

Organization	Materials by Class										Total
	Ag	Al	Cr	Mo	Nb	Ni	Steel	Ti	TiAl	Other	
WUD 49 (UES)		2							2		4
WUD 55 (UES)			1	2	6				48		57
WL/ML								1			1
WL/MLI								1			1
WL/MLIM		15						5			20
WL/MLLM		18						4	8		30
WL/MLLN		1						16	16	6	39
WL/MMC		12									12
Ohio State University									2		2
Wright State University		2							4		6
Virginia Technology								7	1		8
U.S. Army		6									6
U.S. Navy								1			1
CMW	2										2
Lanxide Corp.		26									26
McDonnell Douglas								13		1	14
Pratt & Whitney - Florida						6					6
Pittsburgh Materials Tech.				4						3	7
Vangura Tool				2							2
Total	2	82	1	8	6	6	0	48	81	10	244

5.2 Forging

The 1000-ton Erie forge press was used for plasticity studies, process development and simple upsettings. Table 5-2 summarizes the forging work. Detailed records are on file in the MPL office.

Table 5-2: Summary of Forging Operations

Organization	Alloy System						Total
	Al	Ni	Steel	SS	Ti	TiAl	
WUD 49	49	13	2	3	45	56	158
WUD 52,55,56						28	28
UDRI						2	2
Systran	2						2
MLIN			10		17		27
TOTAL	51	13	12	3	62	76	217

5.3 Rolling

A total of 265 multipass rolling operations were performed. Table 5-3 summarizes the operations. Detailed records are on file in the MPL office.

Table 5-3: Summary of Rolling Operations

Organization	Materials by Class							Total
	Al	Nb-Ti	Ti-Al	Ni	Ti	Al-Li	Other	
WUD 49			57	25	12	23	5	122
WUD 52,55,56	4	1	9		11			25
WL/MLLP					4			4
UDRI							1	1
Wright State Univ.	1				73			74
Univ. of Virginia	1							1
General Electric				5				5
McDonnell Douglas			4		11			15
Lanxide	15							15
Ohio Advanced Tech.							3	3
Total	21	1	70	30	111	23	9	265

5.4 Mechanical Testing

Mechanical testing was performed to provide material data for process modeling and to assist in process development. The majority of the mechanical tests were performed on a 55kip MTS test frame to measure flow stress over a range of temperature and strain rate. A 200kip MTS test frame was also used to conduct heat transfer experiments. Mechanical tests are summarized in Table 5-4.

Table 5-4: Summary of Mechanical Testing

Organization	Compression Tests	Heat Transfers	Total
WUD 49	269		269
WUD 55	6		6
General Electric	178	16	194
Masco	24		24
General Motors	16		16
Caterpillar	8		8
Wyman Gordon	6		6
Navy	4		4
Total	511	16	527

5.5 Evacuation and Degassing

A total of 382 evacuation, degassing and sealing operations were performed on extrusion, forge, heat treatment, HIP and rolling cans. Summaries of these operations by Type of Can are given in Table 5-5. Detailed records of each operation are on file in the MPL office.

Table 5-5: Summary of Evacuation, Outgassing and Sealing Operations

Organization	Type of Can					Total
	Extrusion	Forge	Heat Treat	HIP	Rolling	
WUD 49	19	12		109	9	149
WUD 52,55,56	46	9		111	11	177
UDRI				20		20
McDonnell Douglas	15					15
MLI				1		1
Virginia Tech.	8					8
MLBT				2		2
Allison	4					4
WL/POOX-2				4		4
Systran	2					2
TOTAL	94	21	0	247	20	382

5.6 Vacuum Arc Melting (Button Melts)

A total of 585 Vacuum Arc Melting operations were performed primarily in support of alloy development work by Government and Contract scientists in the Wright Laboratory. These were mainly 50 to 250 gram button and cigar melts. Table 5-6 summarizes these operations by material class and customer. Detailed records are on file in the MPL office.

Table 5-6: Summary of Vacuum Arc Melting

Organization	Material Class							Total
	Au	Cr	Mo	Nb	Ti	TiAl	Other	
WUD 49		14		169		59	8	250
WUD 55,56			13			112	172	297
WL/ML					2			2
WL/MLL			16					16
SAF	2							2
Wright State Univ.							16	16
Other					2			2
Total	2	14	29	169	4	171	196	585

5.7 Vacuum Induction Melting (VIM)

A total of 15 Vacuum Induction Melts (VIM) were performed. These were conducted for solidification research and for alloy development. Many were instrumented with multiple thermocouples so that cooling curves could be compared to results of simulation modeling or interface heat transfer coefficients calculated.

Table 5-7 summarizes these operations. Detailed records are on file in the MPL office.

Table 5-7: Summary of Vacuum Induction Melting

Organization	Material Class		Total
	Al-6Cu-.2Zr-.1Ti-xxx	Ti-6-4	
U.S. Army Research Lab	11		11
Howmet Corp.		4	4
Total	11	4	15

5.8 Heat Treatment

Nearly all of the hundreds of extrusion, forging and rolling operations that were performed required preheats to bring the billets up to the working temperature. In addition to these preheat operations, there were 275 heat treatments performed that were not direct precursors to forming operations. Table 5-8 summarizes the operations. Detailed records are on file in the MPL office.

Table 5-8: Summary of Heat Treat Operations

Organization	Type of Specimens						Total
	Ti	Ti-Al	Ni	SS	Al-Li	Steel	
WUD 49	153	47	1	7	7	2	217
WUD 52,55,56		26					26
Wright State Univ.	5	11					16
General Electric	4		7			5	16
Total	162	84	8	7	7	7	275

5.9 Welding and Fabrication

Welding and fabrication operations were performed in support of metal working operations and equipment maintenance. The bulk of the machining and welding is the making of vacuum tight cans that contain either powder or solid research materials to be extruded, rolled, forged or HIP'ed. Cans are fabricated from a variety of materials, most commonly titanium, stainless steel, carbon steel, or aluminum. Exotic materials and welds are occasionally required, such as the welding of C.P. titanium to TiAl. Every can that is fabricated is tested for vacuum tightness using a helium leak detector. A summary of the major research welding operations is given in Table 5-9.

Table 5-9: Summary of Welding Operations

Organization	Type of Welding Operations						Total
	Extrusion Cans	HIP Cans	Rolling Cans	Forging Cans	ECAE Cans	Other	
WUD 49	16	175	77	59	51	47	425
WUD 52,55,56	39	75	1	28		84	227
UDRI		25				10	35
MLBT		2					2
MLPJ		1					1
WL/POOX-2		10					10
McDonnell Douglas			3				3
Wright State Univ.	5					1	6
Total	60	288	81	87	51	142	709

6. Foundry Move

The first several months of this contract's effort was spent on completing the relocation of the Materials Processing Laboratory (MPL) from Building 51 to Building 655. Old laboratory equipment was refurbished, new equipment was purchased, and necessary modifications were made to the facility. Actual hookup of electric, water and air to the laboratory equipment was begun in June 1992, when Civil Engineering officially turned the High Bay over to us. Among the major tasks performed were:

1. Hooked up utilities to furnaces, pumps, power supplies, welders, and machine tools.
2. Performed startup maintenance on all equipment, such as installing new globars in furnaces and replacing filters, hoses, seals and ion gages on pumps.
3. Extended reach and re-certified 1 ton jib crane as a $\frac{3}{4}$ ton capacity.
4. Purchased and installed new induction generator for the Extrusion Billet Heater.
5. Purchased and installed new induction generator for the Vacuum Induction Melter.
6. Purchased an 8000 lb. fork lift truck for installing forge press tooling.
7. Purchased and installed stairway to top of Erie forge press.
8. Designed and fabricated steel framework and cover for the forge press pit to support a forklift plus 5000 lb. block of tooling.
9. Subcontracted the installation of a 1 ton monorail overhead crane above the forge press.
10. Installed two new induction generators supplied by Erie for forge press.
11. Unpacked all of the supplies, parts and materials from the old laboratory and loaded into newly purchased cabinets.

The new 1000 ton Erie forge press and modernized 700 ton Lombard extrusion press were also tested out and debugged during the last half of 1992. UES personnel conducted an

extensive program to test out the performance of the new presses and to validate the accuracy of the control and data acquisition systems. Several major problems were discovered and diagnosed. These included:

1. A software error in the data acquisition systems on both presses that consistently misrepresented the ram velocity.
2. A design problem in the data acquisition systems that resulted in prohibitively long times to save experimental data.
3. The 1000 ton load cell supplied with the forge press was off by a factor of 2.

UES had these problems corrected by the press suppliers.

By the end of 1992, the Materials Processing Laboratory was fully functioning. All of the equipment relocated from Building 51 was operational and many newly acquired pieces of equipment had greatly enhanced the capabilities of the laboratory.

7. Operation of Materials Processing Laboratory

A major effort of this program is the operation, maintenance and upgrading of the Materials Processing Laboratory (MPL). During the current contract, the relocation of the laboratory from Building 51 to Building 655 was completed. A fundamental shift occurred in the character of the work performed by contract technicians away from being exclusively focused on the operation of metal working equipment toward a broader range of research support jobs. At the same time the operational complexity and maintenance requirements of the forge and extrusion presses increased dramatically. Several new pieces of equipment were added to the contract's "arsenal", including a 55 kip MTS test frame, a 200 kip MTS test frame, a salt bath furnace and environmental chambers for the 200 kip MTS and 1000 ton forge press. The most notable equipment upgrades are noted below.

7.1 *Isothermal Forging Chamber and Tooling*

The potential applications for the 1000 ton Erie forge press would be greatly enhanced by the addition of hot die and isothermal forging capabilities. This would expand the utility of the press in process development for new materials and novel forming processes and allow the subscale modeling of complex, high temperature forming operations.

In May 1992, the Government requested that additional materials be purchased for the fabrication of: (1) a hot die forging tooling stack, (2) an isothermal forging tooling stack, (3) an environmental chamber, and (4) a billet manipulator.

The design concept was based upon an isothermal forging system used by Cameron Iron. Substantial changes had to be made to take into account the different press tonnages and the fact that the Cameron press has a bottom mounted main ram, whereas our press has a top mounted

ram. Detailed design work was done by UES engineers and technicians. Machine drawings and materials lists were completed in September 1993. Materials and parts were purchased. Machining and fabrication was begun by the Zone Shop in Building 5 in November 1993. UES personnel worked closely with the machine shop throughout the fabrication process and handled subcontracting for machining that was beyond the capability of the Zone Shop.

The majority of the machining and fabrication was completed by March 1995 at which point we were ready to begin installation of the tooling, chamber and manipulator and begin fabrication of required subsystems such as heating, argon and hydraulics. Some concern was raised by the Government about the impact that this installation would have on manpower available for ongoing research activities, so the level of effort was restricted to two to three men working in the mornings only. This was later cut back to two men working 1 day a week.

The purchasing of materials and the machining and fabrication of the tooling, chamber, and billet manipulator were all successfully completed. The billet manipulator and the majority of the chamber itself were installed.

Major tasks that must be completed before the forge press has an operational isothermal forging capability include:

1. Completion of chamber roof installation;
2. Design, fabrication and installation of induction coil mounting system;
3. Design, fabrication and installation of argon system;
4. Design, fabrication and installation of hydraulic supply and control system for manipulator;
5. Design, fabrication and installation of work platform for loading billets; and
6. Relocation of large extrusion furnace to permit fork lift access to front of press and reinforcing steel floor plates to handle fork lift loads.

7.2 200 Kip Test Frame and Heat Transfer Measurement System

A critical parameter in many material forming operations and applications is the rate of heat transfer across an interface. In non-isothermal forming operations, the interface heat transfer coefficient can be a dominant parameter because of the effect that temperature loss has on the behavior of the workpiece. In complex composites, such as foil-fiber-foil layups, the resistance of the interfaces to heat transfer is a key design factor.

A 200 kip MTS test frame was setup in the MPL and equipped for precise heat transfer experiments. The basic test frame was relocated from another building and installed in the MPL. Extensive upgrades were required to prepare it as a heat transfer measurement system. The hydraulic control system was upgraded in order to achieve a faster one shot ram speed at full load capacity. A PC based computer control and data acquisition system was added to control the ram speed and acquire multi-channel thermocouple data at high speed. An instrumented tool stack was designed, fabricated and installed. The working dies were fitted with rapid response thermocouples at precise locations below the die surface. Band heaters were installed to heat one or both dies as desired.

The system was successfully used on several projects. In a composite program, the heat transfer from a hot die to a cold die with an intervening foil-fiber-foil layup was measured and used to estimate the resistance of the layup to heat conduction. In a more conventional metal alloy program, the interface heat transfer coefficient was calculated from hot ring tests.

7.3 55 Kip Test Frame and Hot Compression Test Setup

A 55 kip MTS test frame was installed and equipped for constant strain rate hot compression testing. The test frame was fitted with accumulator bottles to increase the load and speed sustainable for a one shot test. An induction generator and coil were installed to provide

die and specimen heating. A tool stack was installed using a Danley die system for alignment. A PC based control and data acquisition system was installed. The UES software HOTCOMP™ was installed to achieve constant strain rate control and rapid data reduction for large test matrix sets.

The installation of the hot compression test system suffered some frustrating delays due to the sharing of equipment (induction generator and hydraulic pumps) with other groups in the building. Nonetheless, when the system was fully installed and operational, it proved to be a real workhorse. Hundreds of hot compression tests were successfully performed.

7.4 Salt Pot Furnaces

The government in-house research program had a critical need for a salt pot furnace for rapid heating of specimens. This requirement is expected to continue in the future. To solve the immediate need, a temporary salt pot furnace was set up on a roll away table in the spray coating booth. This system was troublesome and unreliable, but got the job done at the time. Simultaneously, a more permanent solution was pursued. The old Chambers arc melter was removed from the MPL and plans were drawn up for a permanent salt pot booth in its place. A larger capacity Globar furnace and alumina crucibles were procured. At the conclusion of this contract, the only step was for Civil Engineering to give the go ahead on the hookup of the ductwork.

7.5 Computerized Extrusion Database

For the past 35 years, detailed records have been kept on every extrusion that has been performed in the MPL. This is a wealth of knowledge on the processing of a broad range of materials. Unfortunately, locating relevant information in those records relied upon a technician or scientist recalling the approximate year when the work was done and then going back and

searching through the file cabinets. Work that had been performed before the tenure of current personnel was lost for all practical purposes.

In order to preserve the information in the extrusion records and to facilitate searching for relevant data, all 35 years of extrusion records were entered into a computerized database using Microsoft Access. The database was carefully designed so as to facilitate searches and to reduce data entry errors.

The value of having the extrusion records in a computerized database was demonstrated on the cooperative program with USDOE. That work required the extrusion of a variety of refractory alloys. No one currently at the MPL recalled any previous work on those alloys. A quick look at the computerized database turned up extrusion records on many of the identical alloys, from 34 years ago!